Article

Cell

Combined Social and Spatial Coding in a Descending Projection from the Prefrontal Cortex

Malavika Murugan,[1] Hee Jae Jang,[1] Michelle Park,[1,2] Ellia M. Miller,[1] Julia Cox,[1] Joshua P. Taliaferro,[1] Nathan F. Parker,[1] Varun Bhave,[1] Hong Hur,[4] Yupu Liang,[4] Alexander R. Nectow,[1] Jonathan W. Pillow,[1,2,3] and Ilana B. Witten[1,2,5,*]

[1]Princeton Neuroscience Institute

[2]Department of Psychology

[3]Center for Statistics and Machine Learning

Princeton University, Princeton, NJ 08544, USA

[4]CCTS Bioinformatics Program, The Rockefeller University, New York, NY 10065, USA

[5]Lead Contact

*Correspondence: iwitten@princeton.edu

https://doi.org/10.1016/j.cell.2017.11.002

SUMMARY

Social behaviors are crucial to all mammals. Although the prelimbic cortex (PL, part of medial prefrontal cortex) has been implicated in social behavior, it is not clear which neurons are relevant or how they contribute. We found that PL contains anatomically and molecularly distinct subpopulations that target three downstream regions that have been implicated in social behavior: the nucleus accumbens (NAc), amygdala, and ventral tegmental area. Activation of NAc-projecting PL neurons (PL-NAc), but not the other subpopulations, decreased the preference for a social target. To determine what information PL-NAc neurons convey, we selectively recorded from them and found that individual neurons were active during social investigation, but only in specific spatial locations. Spatially specific manipulation of these neurons bidirectionally regulated the formation of a social-spatial association. Thus, the unexpected combination of social and spatial information within the PL-NAc may contribute to social behavior by supporting social-spatial learning.

INTRODUCTION

A common social behavior in mice and other rodents is the tendency to investigate novel same-sex conspecifics, a behavior characterized by sniffing and grooming. This investigation behavior is typically rewarding, as evidenced by the fact that mice are likely to return to the location in which they previously encountered a conspecific (Panksepp and Lahvis, 2007; Pearson et al., 2012) and that the behavior generates release of dopamine in the nucleus accumbens (NAc) (Gunaydin et al., 2014; Aragona et al., 2006; Gingrich et al., 2000).

Despite the robust and rewarding nature of social investigation, understanding its neural basis has been challenging, in part due to the complexity of the underlying circuitry. In mice, a large number of distributed, but interconnected, brain areas have been implicated, including the prelimbic cortex (PL, part of the medial prefrontal cortex) and several of its projection targets (e.g., the amygdala, ventral tegmental area, and NAc) (Okuyama et al., 2016; Wong et al., 2016; Lin et al., 2011; Hitti and Siegelbaum, 2014; Yizhar et al., 2011; Lee et al., 2016a; van Kerkhof et al., 2013; Takahashi et al., 2014; Wang et al., 2011; Bicks et al., 2015; Gunaydin et al., 2014; Felix-Ortiz et al., 2016; Amadei et al., 2017).

In particular, activation of the PL causes mice to spend significantly less time investigating a conspecific, suggesting an important role of this region in social preference (Yizhar et al., 2011). However, inhibition of the endogenous activity in the same region results in no observable change in social preference (Yizhar et al., 2011). This discrepancy raises the possibility that experimental activation of PL reduces social investigation by producing unnatural patterns of activation of projection targets, rather than by replicating activity that occurs endogenously during the behavior (Otchy et al., 2015).

To address this possibility, and more broadly to clarify the nature of PL's contribution to social investigation behavior, we manipulated and recorded from projection-defined subpopulations of PL neurons. We first sought to determine which descending projection from PL impacts social investigation when activated. We found that activation of PL neurons that project to the NAc decreased social investigation, while other descending projections from PL did not have this effect. We then examined if and how the endogenous activity within the NAc-projecting PL (PL-NAc) subpopulation is modulated by social investigation. Cellular resolution imaging revealed that many neurons were active during social investigation, but surprisingly, this activity depended on the location of the social encounter. Based on this finding, we manipulated the activity in PL-NAc neurons in a spatially specific manner. This experiment was motivated by the hypothesis that the combined social-spatial code in these neurons could guide social behavior by governing

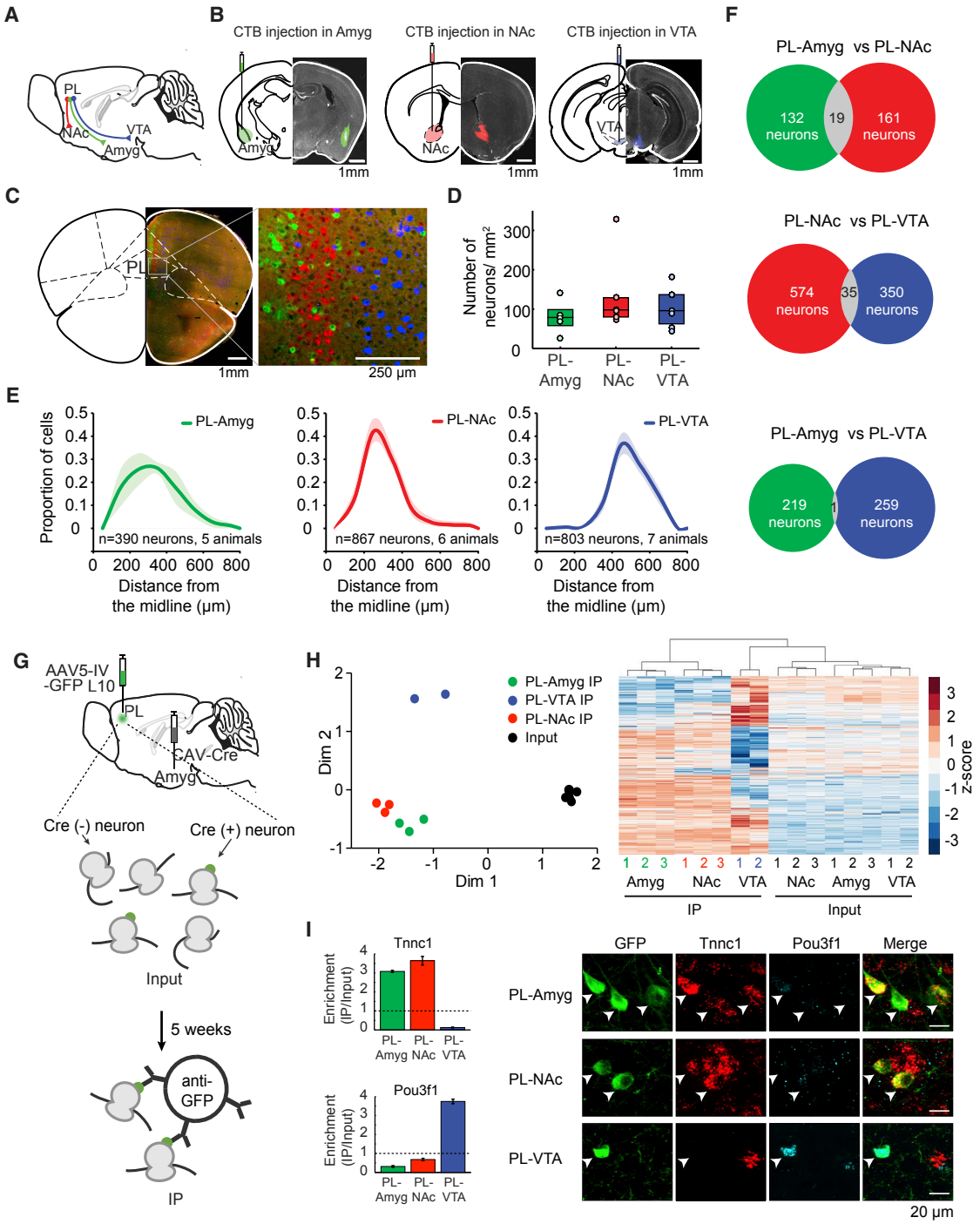

Figure 1. Anatomically and Molecularly Distinct Subpopulations of PL Neurons Project to the NAc, VTA, and Amyg

(A) Schematic of the mouse brain with subcortical projections of the PL to the Amyg (green), NAc (red), and the VTA (blue).

(B) Each brain section includes a schematic (left) and the histology (right) of cholera toxin subunit B (CTB) targeting to the Amyg (left panel), the NAc (center panel), and the VTA (right panel). Scale bar, 1 mm.

(C) A coronal section of retrogradely labeled neurons in PL from CTB injections in Amyg (green), NAc (red), and VTA (blue). 2.2-m anterior bregma. Scale bar, 1 mm in main panel, 250 μm in inset.

(D) A similar number of PL neurons labeled with CTB from Amyg, NAc, and VTA injections. (Mean ± SEM: 134 ± 40 neurons/mm^2 for NAc; 80 ± 17 for Amyg; and 105 ± 20 for VTA; $p = 0.43$ for 1-way ANOVA comparing cell density between the subpopulations). In the boxplots, the center indicates the median, and the bottom and top edges indicate 25th and 75th percentiles, respectively.

(legend continued on next page)

the formation of social-spatial associations, perhaps through synaptic plasticity in the NAc. Consistent with this hypothesis, spatially specific manipulation of these neurons during social investigation bidirectionally regulated the formation of a preference for the location of a social encounter. Thus, PL-NAc neurons encode a combination of social and spatial information which appears to support learning to associate a spatial location with a social encounter.

RESULTS

Anatomically and Molecularly Distinct Neurons Project from PL to the NAc, VTA, and Amygdala

To address the nature of PL's control over social behavior, we first asked if distinct subpopulations of neurons within PL target major downstream regions that have themselves been implicated in social behavior (Gunaydin et al., 2014; Felix-Ortiz et al., 2016; Dölen et al., 2013; Heidbreder and Groenewegen, 2003; Carr and Sesack, 2000; Berendse et al., 1992). To this end, retrograde tracers were injected into the NAc, amygdala (Amyg), or ventral tegmental area (VTA) to enable visualization of PL neurons that project to each target region ("PL-NAc," "PL-Amyg," and "PL-VTA" subpopulations; Figures 1A–1C and S1A, n = Amyg: 390 neurons from 5 animals, NAc: n = 867 neurons, from 6 animals, VTA: n = 803 neurons from 7 animals). We observed a similar density of PL-NAc, PL-Amyg, and PL-VTA neurons within the PL (Figure 1D; mean ± SEM: NAc: 134 ± 40, Amyg: 80 ± 17 and VTA: 105 ± 20 neurons/mm^2; $p = 0.43$ for 1-way ANOVA of cell density between the subpopulations). However, the 3 subpopulations occupied different cell layers, with the PL-NAc neurons positioned more medially than the PL-VTA neurons and the PL-Amyg neurons distributed more broadly than the other two subpopulations (Figures 1C and 1E, Kolmogorov-Smirnov [K-S] test to compare medial-lateral [M/L] distribution of the 3 populations in a pairwise manner, $p < 0.0001$ for all 3 comparisons, Bonferroni-Holm corrected; M/L cell distributions at 3 A/P locations in Figure S1B). Consistent with the distinct laminar distributions, there was little overlap at the single cell level between the 3 subpopulations, as assessed by co-labeling of multiple retrograde tracers, indicating that PL-NAc, PL-Amyg, and PL-VTA neurons are anatomically distinct subpopulations (Figure 1F; neuron overlap: NAc-Amyg, 6.09% or 19/312 from 2 animals; NAc-VTA, 3.65% or 35/959 from 3 animals; and Amyg-VTA, 0.21% or 1/479 from 2 animals).

To further compare PL-NAc, PL-Amyg, and PL-VTA neurons, we performed RNA sequencing (RNA-seq) on each population using the projection-specific molecular profiling technology Retro-TRAP (translating ribosome affinity purification) (Nectow et al., 2015, 2017b; Ekstrand et al., 2014) (Figures 1G and S1C). This revealed significant differences in enrichment levels in 2,745 out of 15,041 genes examined (Figure 1H; Table S1; $p < 0.01$, 1-way ANOVA adjusted for multiple comparisons). Visual inspection of individual replicates, through both multidimensional scaling and hierarchical clustering, further supported the conclusion that the three PL projection populations are distinct, as it revealed more similarity for replicates within each population than across populations (Figure 1H). Interestingly, PL-VTA was much more molecularly distant from the other 2 populations (Figure 1H). Considering that there is minimal single-cell overlap between any of the 3 populations (Figure 1F), but considerable laminar overlap between PL-NAc and PL-Amyg (Figure 1E), together this suggests that the laminar distribution may be a major predictor of molecular phenotype.

To validate the molecular phenotyping, we examined the laminar distribution of 4 marker genes that differentiated these projection populations using the Allen Brain Atlas database (Lein et al., 2007), which allowed us to compare the laminar distribution of each marker gene to the laminar distribution we had identified from each subpopulation (genes *Dkkl1*, *Ngb*, *Fam84b*, and *Fezf2*; Figure S1D). As an additional form of validation, we confirmed projection-specific expression of two of the top differentially expressed genes across treatments, *Tnnc1* and *Pou3f1*, by comparing fluorescence *in situ* hybridization (FISH) with projection-specific labeling (Figure 1I). Further validating these findings, our RNA-seq results replicated the major hits reported in a recent microarray study (Kim et al., 2017) that compared expression between PL-NAc and PL-VTA neurons (>2.8-fold preferential enrichment for *Nptx2*, *Nrn1*, and *Sccpdh* in PL-NAc; and >2.7-fold preferential enrichment for *Bcl11b/CTIP2*, *Chst8*, and *Tcerg1l* in PL-VTA; Table S1).

(E) Quantification of the M/L distribution of PL-Amyg (green), PL-NAc (red), and PL-VTA (blue) neurons. Shading denotes SEM. The 3 subpopulations are distributed differently (Kolmogorov-Smirnov [K-S] test to compare M/L distribution of the 3 populations in a pairwise manner, $p < 0.0001$ for all 3 comparisons, Bonferroni-Holm corrected).

(F) Little overlap between the 3 projection populations at the individual cell level (neuron overlap: NAc-Amyg, 6.09% or 19/312 neurons from 2 animals; NAc-VTA, 3.65% or 35/959 from 3 animals; and Amyg-VTA, 0.21% or 1/479 from 2 animals).

(G) The experimental design for projection-specific RNA-seq with Retro-TRAP. Top to bottom: schematic of injection of retrogradely transported CAV-Cre in the Amyg and Cre-dependent AAV5 IV-GFPL10 virus in PL, followed by a 5-week expression period to allow for incorporation of GFPL10 fusion protein into ribosomes of Cre(+) neurons. The ribosomes tagged with GFP were then immunoprecipitated with GFP antibodies, and the immunoprecipitated (IPs) RNA was quantified.

(H) Multidimensional scaling and hierarchical clustering. Left: a multidimensional scaling plot (plotMDS function of the limma R package) of the RNA-seq data of the three PL projection populations (n = 3 replicates of 6 mice each for PL-Amyg and PL-NAc and n = 2 replicates of 6 mice each for PL-VTA). Right: hierarchical clustering of the logCPM (counts per million) of the top variant genes with IP enrichment (based on 724 genes with log fold change >0 in at least one of the projections) demonstrates differential expression of genes across the IPs and inputs of the three PL projection populations. Color is scaled based on a row-wise *Z* score of the logCPM.

(I) Left: *Tnnc1* and *Pou3f1*: RNA-seq comparison (counts per million IP/counts per million input; mean ± SEM) across the three populations. Right: fluorescence *in situ* hybridization (FISH) of the Tnnc1 (red) and Pou3f1 (cyan) with viral labeling of the three projection populations (green). PL-NAc and PL-Amyg neurons expressed *Tnnc1*, whereas PL-VTA neurons expressed *Pou3f1*.

See also Figure S1 and Table S1.

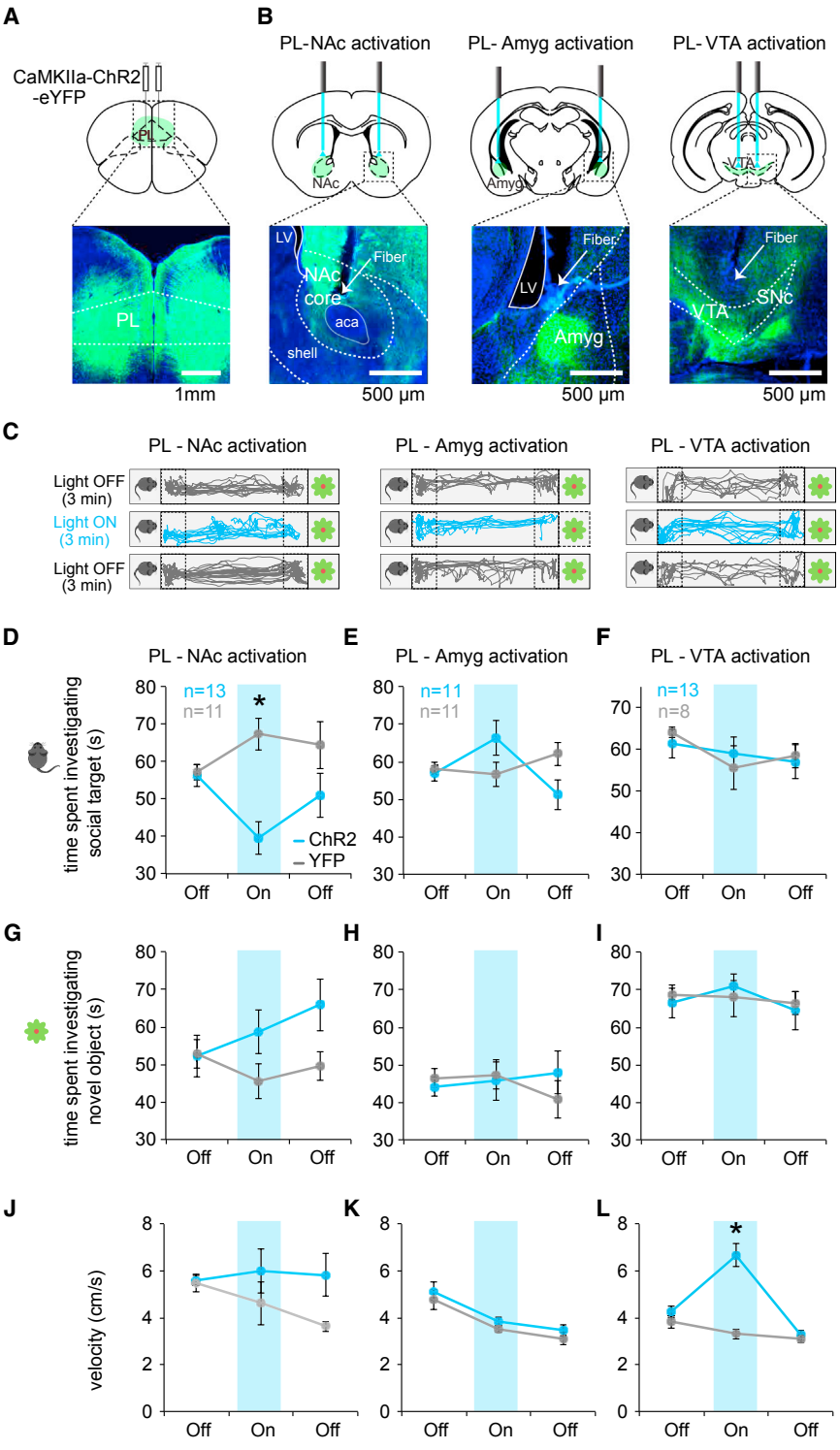

Figure 2. In the Linear 3-Chamber Assay, Activation of PL-NAc Neurons, but Not PL-VTA or PL-Amyg Neurons, Results in Decreased Social Preference

(A) A schematic (top panel) and coronal brain slice (bottom panel) of AAV5 CaMKIIa-ChR2-YFP injection in PL.

(B) Schematic (top panel) and histology (bottom panel) of fiber placement and terminal expression of ChR2-YFP in NAc, Amyg, and VTA.

(C) Position tracking from representative mice receiving activation of PL-NAc (left), PL-Amyg (center), or PL-VTA (right), while exploring the 3-chamber arena pre-stimulation (top panel), stimulation (middle panel, 447-nm blue light, 20-Hz stimulation, 5-ms pulse duration, 7 mW), and post-stimulation (bottom panel). Time spent near the social target or novel object (demarcated by dotted line) was measured.

(D) Activation of PL-NAc terminals decreased the amount of time mice spent in proximity of the social target (ANOVA with group, epoch, and light as factors; $p = 0.0196$ for group X light).

(E and F) Activation of PL-Amyg (E) and PL-VTA (F) terminals had no effect on time spent in proximity of the social target ($p = 0.128$ for group X light for PL-Amyg and $p = 0.406$ for PL-VTA).

(G–I) Activation of PL-NAc (G), PL-Amyg (H), and PL-VTA (I) terminals had no effect on time spent in proximity of the novel object ($p = 0.579$ for group X light for PL-NAc, $p = 0.625$ for PL-Amyg, and $p = 0.485$ for PL-VTA).

(J and K) Activation of PL-NAc (J) and PL-Amyg (K) terminals had no effect on velocity ($p = 0.111$ for group X light for PL-NAc, $p = 0.926$ for PL-Amyg).

(L) Activation of PL-VTA neurons resulted in a large and significant increase in velocity ($p < 0.0001$ for group X light).

Error bars indicate SEM (D–L).

See also Figure S2.

Activation of PL-NAc Neurons, but Not PL-VTA or PL-Amyg Neurons, Decreases Social Investigation in the Linear 3-Chamber Assay and Home-Cage Assay

Given that PL is composed of anatomically and molecularly distinct subpopulations that target the NAc, VTA, and Amyg, we next asked if the previously reported effect of PL activation on social preference (Yizhar et al., 2011) is broadly distributed across these descending projections, or if it can be localized to a specific projection. To address this question, we transiently activated PL-NAc, PL-Amyg, or PL-VTA neurons through ChR2 stimulation, while assessing social behavior using a 3-chamber test. To this end, an adeno-associated virus type 5 (AAV5) expressing either ChR2-YFP or YFP only (control mice) was injected into the PL (Figure 2A), and optic fibers were implanted above the NAc, VTA, or Amyg (Figure 2B; fiber placement summary in Figure S2A). Before performing the 3-chamber test, the efficacy of optogenetic terminal activation was verified with *in vivo* electrophysiology (Figures S2B–S2F). During the behavioral test, mice explored a linear 3-chamber arena containing an encaged juvenile stranger

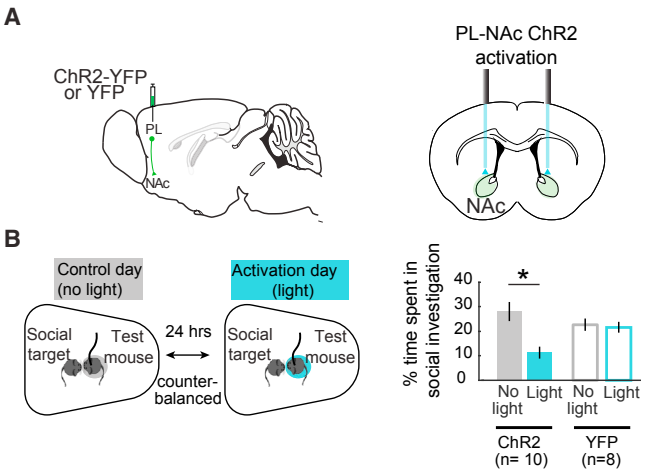

Figure 3. In the Home-Cage Assay, Activation of PL-NAc Neurons Results in Decreased Social Investigation

(A) Schematic of AAV5 CaMKIIa-ChR2-YFP injection in PL (left) and fiber placement targeting NAc terminals.

(B) Left: schematic of the experimental design. Mice investigated novel social targets in their home-cage across 2 days. A control day with no stimulation was counterbalanced with another day with stimulation (473-nm blue light, 10-Hz stimulation, 5-ms pulse duration, 1.5 mW). Time spent investigating the social target was scored. Right: activation of PL-NAc terminals decreased the amount of time mice spent in social investigation (ANOVA with groups-ChR2/YFP and days-light/no light as factors, group X days $p = 0.0071$, post hoc paired t test comparing the ChR2 group across days, $p = 0.0018$). Investigation was defined as epochs when the mouse was engaged in pursuit, sniffing, or grooming of the social target (see the STAR Methods).

Error bars denote SEM. See also Figure S3.

mouse in one side-chamber (the "social target") and an encaged novel object on the other side-chamber, with and without optogenetic stimulation (protocol: 3 min of no light, followed by 3 min of light, followed by 3 min of no light; Figures 2C and S2G). Optogenetic activation of PL-NAc neurons resulted in a decrease in the amount of time mice spent near the social target, mimicking prior findings based on non-selective activation of PL neurons (Yizhar et al., 2011) (Figure 2D; ANOVA with group, epoch, and light as factors; $p = 0.0196$ for group X light; Figure S2J). This decrease in social preference was mediated by a decrease in the duration of each social investigation bout (Figure S2H, $p = 0.049$, ANOVA group X light interaction), rather than an increase in the interbout interval (Figure S2H, $p = 0.505$, ANOVA group X light interaction). In contrast with the decrease in social preference, there was no decrease in novel object preference or preference for the rest of the chamber when PL-NAc neurons were stimulated, and in fact there was a trend toward increased novel object and the rest of the chamber preference (Figure 2G, $p = 0.579$ for group X light; Figure S2I).

In contrast to stimulation of PL-NAc neurons, stimulation of PL-Amyg and PL-VTA neurons had no effect on social target preference (Figures 2E and 2F; $p = 0.128$ for group X light for PL-Amyg and $p = 0.406$ for PL-VTA) or novel object preference (Figures 2H and 2I; $p = 0.625$ for group X light for PL-Amyg and $p = 0.485$ for PL-VTA), pointing to a unique contribution of PL-NAc neural activity in supporting social preference.

To determine if the decrease in social preference mediated by PL-NAc stimulation could result from changes in locomotion, we compared the mouse's velocity during the baseline and stimulation epochs in ChR2 and control mice. We did not observe a significant change in the velocity of the mice during stimulation of PL-NAc or PL-Amyg neurons, although there was a trend of increased velocity in the PL-NAc group in the post-stimulation epoch (Figures 2J and 2K; $p = 0.111$ for group X light for PL-NAc, $p = 0.926$ for PL-Amyg). In contrast, activation of PL-VTA neurons resulted in a large and significant increase in velocity (Figure 2L; $p < 0.0001$ for group X light).

Taken together, PL-NAc stimulation caused a change in social preference but not in velocity, while PL-VTA stimulation caused a change in velocity but not social preference. This double dissociation between social investigation and velocity provides compelling evidence that a change in velocity alone cannot explain the decrease in social investigation resulting from PL-NAc stimulation. In addition, the similar density of PL-VTA, PL-NAc, and PL-Amyg neurons (Figure 1D), and the similar proportions of downstream neurons affected by stimulation (Figures S2B–S2F), suggests that the behavioral differences observed by stimulating these 3 projections are unlikely to result from differences in the efficacy of the stimulation.

Given that the 3-chamber test involves an encaged social target, we sought to determine if activation of PL-NAc terminals also reduced social investigation in a more natural assay of social investigation. In the home-cage assay, a novel conspecific was introduced into the home-cage of the test mouse and time spent in social investigation was scored. We found that PL-NAc activation (Figure 3A; fiber placement summary in Figure S3A) resulted in a large and significant reduction in social investigation in this assay as well, consistent with the reduction in social preference in the 3-chamber test (Figure 3B, ANOVA with groups-ChR2/YFP and days-light/no light as factors, group X days $p = 0.0071$, post hoc paired t test comparing the time spent investigating social target on control and stimulation days, $p = 0.0018$; Figure S3B).

Given that activation of PL-NAc neurons decreased social preference in the linear 3-chamber assay and home-cage assay, we sought to determine if inhibition of these neurons affected these behaviors as well. To inhibit PL-NAc neurons, we injected retroAAV-Cre in the NAc and a Cre-dependent NpHR3.0 virus in the PL, and implanted optical fibers over the cell bodies in PL (Figure S3C). Inhibition of PL-NAc neurons resulted in no observed change in social investigation in either the linear 3-chamber assay (Figures S3D and S3E, ANOVA with group and days as factors; $p = 0.397$) or the home-cage assay (Figure S3F, ANOVA with group, light, and epoch as factors; $p = 0.825$ for group X light). These results from PL-NAc manipulations replicates prior results from non-specific PL manipulations (Yizhar et al., 2011), which reported a decrease in social preference when activating PL neurons, but no effect of inhibition. The negative result from PL-NAc inhibition in these assays suggests that the endogenous activity in PL-NAc neurons does not support social preference, and there may instead be another mechanism through which PL-NAc activation contributes to social behavior. To gain insight into this possibility, we sought to record the natural neural dynamics of these neurons during social investigation assays.

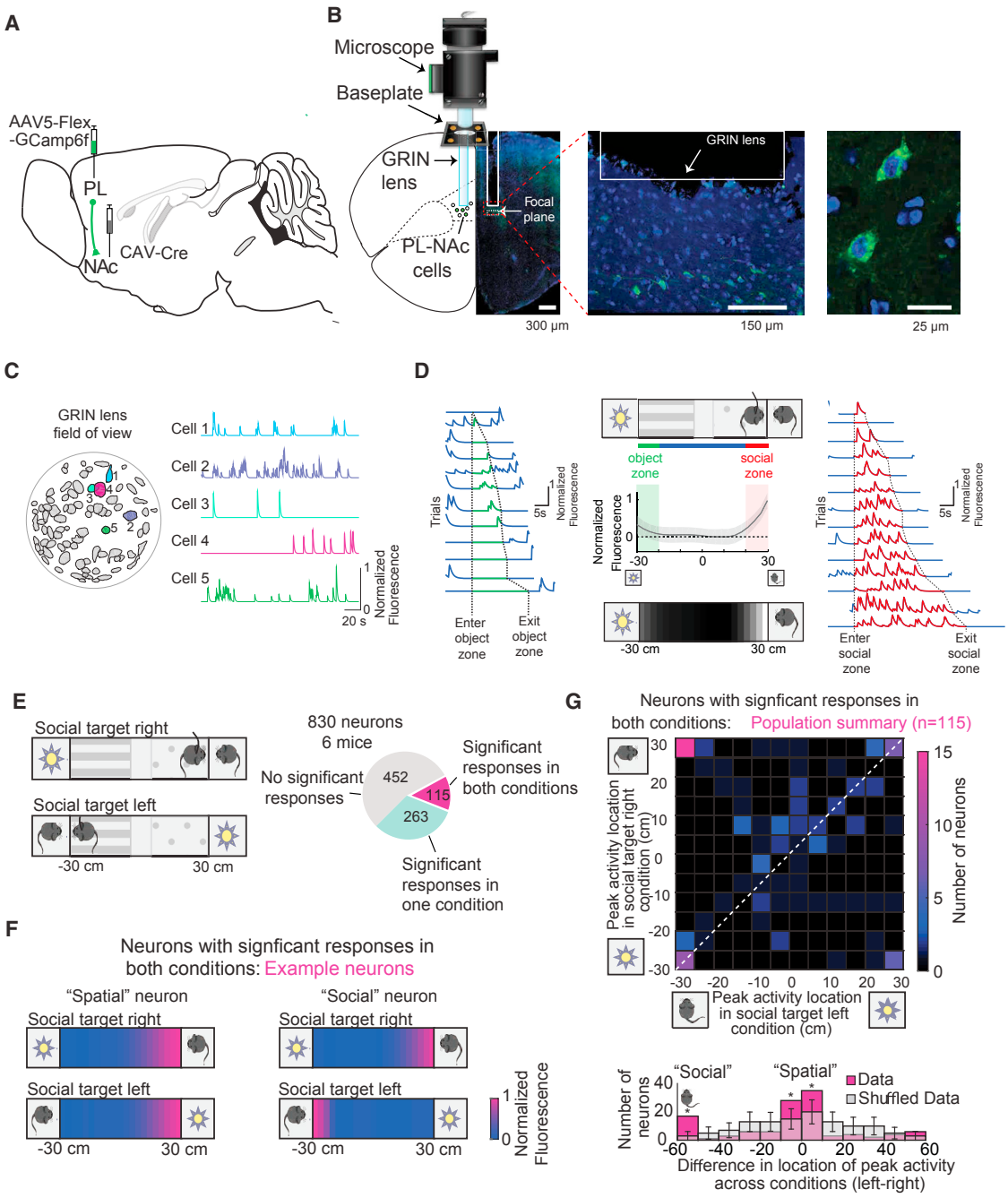

Figure 4. In the 3-Chamber Assay, Some PL-NAc Neurons Are "Spatial" and Others Are "Social"

(A) Targeting of GCaMP6f to PL-NAc neurons. Retrograde CAV-Cre virus was injected in the NAc and Cre-dependent AAV5 GCaMP6f in PL.

(B) Left: GCaMP6f imaging setup and histology of GRIN lens placement in PL. Middle: GCaMP6f expression in PL-NAc neurons in green and DAPI in blue. Scale bar, 150 µm. Right: a confocal image of PL-NAc neurons showing nuclear exclusion of GCaMP6f. Scale bar, 25 µm.

(C) The field of view of a GRIN lens in a representative animal with identified neurons demarcated (left panel). The right panel consists of fluorescence traces of example neurons (color-coded in the left panel).

(D) Middle top panel: the imaged mouse explored a linear 3-chamber arena consisting of an encaged social target (novel mouse) on one end and an encaged novel object on the other. Middle central panel: the response field of an example neuron that responds in the proximity of the social target. Shaded regions denote error bars (2 SD). Middle bottom panel: heatmap of the spatial field of the same neuron. Left and right panels: responses in this neuron to individual visits to the social (red) or object (green) zone. Trials organized in ascending order of time spent in each zone.

(E) Mice were imaged while exploring the arena on two consecutive visits: first with the social target in one location (either "social target right" or "social target left") and next with the social target in the other location. Of 830 neurons imaged from 6 mice, 14% (115 neurons) displayed significant responses in both

(legend continued on next page)

PL-NAc Neurons Are Active during Social Investigation in a Manner that Depends on Spatial Location

To identify the endogenous pattern of activity in PL-NAc neurons during social investigation, we expressed the calcium indicator GCaMP6f selectively in PL-NAc neurons by injecting a retrogradely traveling CAV2 virus expressing Cre in the NAc and an AAV5-expressing Cre-dependent GCaMP6f in the PL (Figure 4A). A head-mounted microscope (Ghosh et al., 2011) coupled to a gradient-index (GRIN) lens was implanted above PL to obtain cellular-resolution images of PL-NAc neurons while mice explored the linear 3-chamber arena (Figures 4A and 4B; individual neurons were identified from videos using CNMFe; Figure 4C, example video in Movie S1; Zhou et al., 2016). A total of 830 neurons were imaged in 6 animals, and GRIN lens placement was confirmed post hoc with histology (Figure S4A).

During exploration of the 3-chamber arena, we observed example neurons with elevated activity whenever the imaged mouse was in the vicinity of the social target (example neuron in Figure 4D). However, since the social target is constrained to be in a specific spatial location in this assay, it is essential to distinguish potential social target-related responses from selectivity for the spatial location of the imaged mouse. To distinguish between these possibilities, all mice were imaged while exploring the arena on two consecutive visits (Figure 4E): first with the social target in one location (either "social target right" or "social target left"), and next with the social target in the other location. 14% of neurons displayed significant spatial selectivity in both conditions, while 31% displayed significant spatial selectivity in only one of the two conditions (significance assessed based on cross-validated predictions of activity based on spatial field estimates; see the STAR Methods).

Of the 115 neurons with significant selectivity in both conditions ("social target right" and "social target left"), some neurons exhibited peak responses at a similar spatial location across both conditions (example "spatial neuron" in Figures 4F and S4B), while other neurons responded most strongly near the location of the social target in both conditions (example "social neuron" in Figures 4F and S4C). In contrast, very few neurons responded consistently near the location of the novel object. In the population summary (top panel of Figure 4G), neurons along the diagonal correspond to "spatial neurons" with the same spatial selectivity regardless of the location of the social target, while neurons in the upper left correspond to "social neurons" that respond in the vicinity of the social target, regardless of its spatial location. Across the population, there were more of these "spatial neurons" and "social neurons" than expected by chance (bottom panel in Figure 4G, $p < 0.001$, 1-tailed t test comparing data in each bin to simulated data generated from a spatially uniform distribution of peak responses). Although the "social neurons" provide a compelling neural correlate of social investigation, it is worth noting that they represent a relatively small fraction of the total imaged population (15 of 830, or 1.8%).

Interestingly, examining the population of neurons with significant responses in only one condition ("social target right" or "social target left," Figure 5A), rather than both conditions, revealed a substantially larger fraction of neurons that were active in the vicinity of the social target (90 of 830 neurons, or 10.8%, were most active in the spatial bin adjacent to social target, for one of the two conditions; Figure 5). This is because many neurons exhibited elevated responses in the vicinity of the social target in only 1 of the 2 conditions, and showed no spatial selectivity at any location in the other condition (example neurons in Figure 5B, population summary Figures 5C, S5A, and S5B). This phenomenon was observed for both the 1st and 2nd condition tested, implying that these responses cannot be explained based on greater social target novelty in the 1st condition (6.1% of all neurons responded most strongly near the social target in the first condition, whereas 4.7% did so in the second condition). In summary, many neurons responded in the proximity of the social target in a manner that depended on if it was in the left or right location. This implies that PL-NAc neurons encode the conjunction of social target proximity and spatial location.

We performed several additional control experiments to clarify the robustness of these findings in the linear 3-chamber assay. First, we compared responses in "spatial neurons" in the absence of social targets or novel objects on either end of the chamber. As expected, most of these "spatial neurons" responded in the same location in this new condition as well (Figures S4D and S4E). Additionally, we repeated the same experimental design in new mice with different types of social targets (adult males or estrous females, rather than juvenile males), as well as a different type of novel object (food rather than toy; Figure S5C), and observed similar proportions of the various responses. To further characterize social responses, we examined the impact of the orientation of the imaged mouse relative to the target mouse on neural responses (example neurons in Figures S5D and S5E, population summary in Figure S5F). Finally, to further characterize the social-spatial neurons, we compared responses in social-spatial neurons in the presence of a second social target on the other side of the chamber (Figures S5G–S5I). Taken together, these control experiments support the robustness of our findings of spatial and social-spatial responses.

Although the 3-chamber assay provides a powerful approach to determine that social and spatial responses are combined in individual neurons, the encaged nature of the social target

conditions, whereas 31% (263 neurons) displayed significant responses in only 1 of the 2 conditions. The rest of this figure focuses on the 115 neurons with significant responses in both conditions.

(F) Left: the spatial field of an example "spatial neuron" that exhibited peak responses at a similar spatial location across both conditions (social target right condition on the top and social target left condition on the bottom). Right: the spatial field of an example "social neuron" that responded most strongly near the social target in both conditions.

(G) Population summary of neurons with significant responses across both conditions (n = 115). Top: the number of neurons with peak response at each location across the two conditions. Bottom: the number of neurons as a function of the difference in location of peak activity across the 2 conditions reveals more "spatial neurons" and "social neurons" than expected by chance ($p < 0.001$, 1 tailed t test comparing data in each bin to simulated data generated from a spatially uniform peak distribution).

Error bars denote 2 SDs. See also Figure S4 and Movie S1.

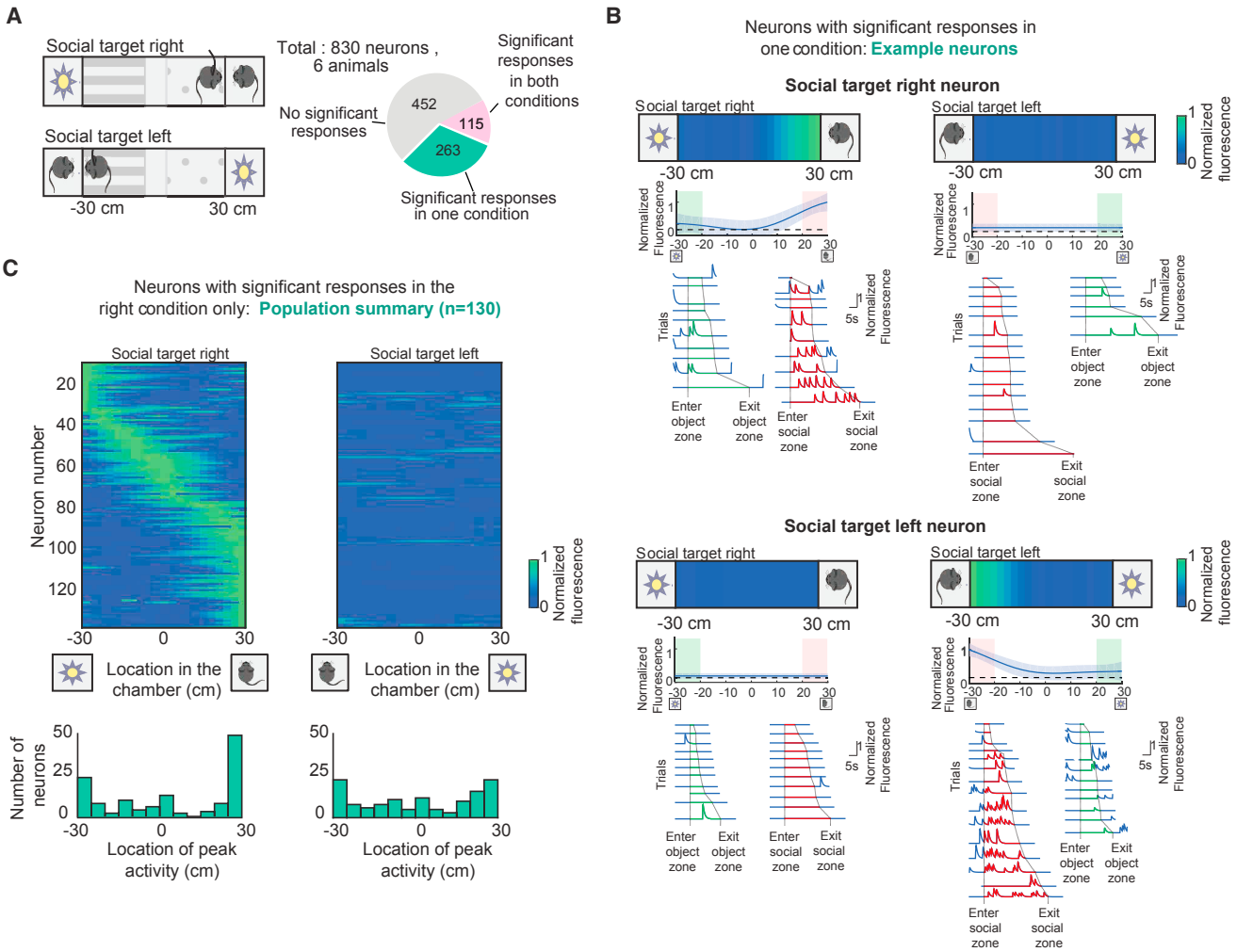

Figure 5. In the 3-Chamber Assay, Many PL-NAc Neurons that Respond Near the Social Target Only Do So in One Spatial Location

(A) This figure focuses on the 263 (out of 830) PL-NAc neurons with significant responses in only one of the two conditions in the imaging experiment in the 3-chamber assay described in Figure 4.

(B) Top panel: example neuron that exhibited spatial selectivity only in the social target right condition. The top row is a heatmap of the response field of the neuron, middle row consists of the response field of the neuron with error bars (2 SD), and the bottom row is comprised of individual visits (trials) to the object (green) and social (red) zones. Bottom panel: example neuron that exhibited spatial selectivity only in the social target left condition.

(C) Top panel: spatial fields of all neurons (n = 130) with significant responses only in the social target right condition (left panel) and not the social target left condition (right panel). Bottom panel: histogram of peak responses of the neurons along the length of the chamber. 38% of neurons responded most strongly in the vicinity of the social target, but only in one of the two spatial locations (in this case social target on the right).

See also Figure S5 and Movie S1.

disrupts natural social interactions. Thus, to determine if PL-NAc neurons respond during social investigations between two freely moving mice, and if such correlates are modulated by spatial location as observed in the 3-chamber assay (Figures 4G and 5C), we imaged 373 PL-NAc neurons during the home-cage assay across 4 mice (Figure 6A, example video in Movie S2). The locations of both mice were tracked and social investigation epochs were manually annotated (defined as periods when the imaging mouse was in pursuit, grooming or sniffing the social target). Some PL-NAc neurons, including the example neurons in Figure 6B, responded during investigation of social targets (Figure 6B). This elevated activity was evident across the neural population during social investigation, but not during investigation of a novel object (Figure S6, $p < 0.0001$, for 1-way ANOVA with investigation of mouse 1, mouse 2, versus novel object as the factor, post hoc Tukey's honest significant difference [HSD] tests; $p = 0.155$ for mouse1 versus mouse 2, $p < 0.001$ for mouse 1 versus novel object, $p < 0.001$ for mouse 2 versus novel object). Taken together, these findings suggest that PL-NAc neurons respond more strongly to social target investigation than novel object investigation.

A striking result from the 3-chamber assay was that many PL-NAc neurons responded in the vicinity of the social target in only one of the two spatial locations that we tested (Figure 5). To

determine if this combined spatial and social code generalized to the home-cage assay, we took advantage of the fact that this assay involves bouts of social investigation interleaved with non-investigation epochs. This allowed us to calculate the spatial selectivity of each neuron during periods of investigation and also during periods without investigation. Comparison of spatial fields of individual neurons across these two conditions revealed modulation by social investigation: for example, some neurons exhibited spatial fields only during social investigation (example neuron in Figure 6C) while others exhibited spatial fields only during epochs without social investigation (example neuron in Figure 6D). To determine if this modulation of spatial fields by social investigation was significant across the PL-NAc population, we compared the predictive power of two models on cross-validated data. One model was based on neurons having the same spatial field regardless of whether or not the mice were interacting (spatial-only model), and the other model was based on calculating a different spatial field during investigation versus during non-investigation epochs (social-spatial model). Across the population, the latter model produced significantly better predictions of neural activity in comparison to a model that only took into consideration spatial location (paired t test comparing the correlation coefficients of the predicted and real data across the two models, $p = 3.41 \times 10^{-37}$, n = 373 neurons). In addition, 73.5% of neurons had activity that was best predicted by the social-spatial model while only 12.6% had activity best predicted by spatial-only model (Figure 6E). Of neurons best described by the social-spatial model, similar fractions increased versus decreased their peak spatial response during investigation (Figure 6F). In summary, these findings demonstrate that PL-NAc neurons encode the conjunction of social and spatial information in the home-cage assay.

Spatially Specific Manipulation of PL-NAc Neurons Bidirectionally Regulates Social-Spatial Learning

What could be the function of a combined social-spatial code in PL-NAc neurons? Given that plasticity of PL synapses in NAc is thought to be a site of reward-related learning (Britt et al., 2012; Otis et al., 2017; McFarland et al., 2003; Pascoli et al., 2014; Lee et al., 2016b), we hypothesized that these neurons could support the formation of social-spatial associations by providing information to the NAc about the location of social encounters. To test this hypothesis, we designed a specialized social conditioned place preference paradigm (social CPP) which involved a test mouse exploring two chambers, each with an encaged social target. This paradigm enabled us to differentially modulate the formation of a social preference for one location, but not for the other (Figure 7C). To selectively inhibit PL-NAc neurons, we used an intersectional virus strategy to express the inhibitory opsin eNpHR3.0-eYFP (or control virus; Figures 7A and 7B and fiber placement summary in S7A). Before conditioning, mice first experienced a baseline day in which there was no social target and no optogenetic stimulation, in order to ensure the mice exhibited no initial spatial bias. They then received two conditioning days in which the neurons were inhibited in the vicinity of one social target but not the other, followed by a final test day to assess persistent changes in spatial preference (Figure 7C). We found that mice that received inhibition of PL-NAc neurons did not form an association with the social zone associated with inhibition (relative to control mice) (Figures 7D and S7B, ANOVA with group and days as factors; p = 0.0271 for group X days, followed by post hoc t test baseline: p = 0.378, cond day 1: p = 0.008, cond day 2: p = 0.025, test day: p = 0.024), while the preference for the social zone without inhibition was indistinguishable from controls (Figure 7E, ANOVA with group and days as factors; p = 0.3416 for group, p < 0.001 for days, p = 0.9851 for group X days). This lack of preference for the social zone associated with inhibition persisted to the next day, suggesting that activity in PL-NAc neurons is necessary for forming a social-spatial preference.

Although these results are consistent with the idea that PL-NAc neurons support the formation of social-spatial associations, it is important to control for the possibility that inhibition of PL-NAc neurons is aversive, and therefore inhibition of those neurons would result in altered spatial preference in the conditioning assay described above (Figure 7C), even in the absence of a social target. To examine this possibility, in a new group of mice we repeated the same conditioning paradigm as described above, inhibiting the PL-NAc neurons in the same zone of the same chamber, but critically, in this case the social targets were omitted (Figure 7F). In this case, inhibition had no effect on spatial preference (Figure 7G, ANOVA with zones and days as factors; p = 0.775 for group X days), supporting the conclusion that inhibition of PL-NAc neurons does indeed disrupt social-spatial learning.

To determine if spatially specific activation of these neurons had the converse effect of inhibition, and serves to enhance learning, we used an analogous viral strategy to express ChR2-eYFP in PL-NAc neurons (or control virus; Figure 7H). The social CPP experiment was performed as before (Figure 7C). We found that spatially specific activation of PL-NAc neurons generated an enhanced preference for the social zone associated with stimulation (Figures 7I–7K, ANOVA with group and days as factors; p = 0.043 for group X days, post hoc t tests for Baseline: p = 0.897, cond day 1: p = 0.011, cond day 2: p = 0.021, test day: p = 0.001). Taken together, these findings suggest that spatially specific manipulation of PL-NAc neurons bidirectionally regulates social-spatial learning, as assayed with a social CPP.

DISCUSSION

Here, we show that PL is composed of distinct populations of neurons that target 3 regions that have been implicated in social behavior: the NAc, VTA, and Amyg. Activation of PL-NAc neurons, but not the other descending projections from PL, decreases social preference across two assays (home-cage assay and 3-chamber assay). In both assays, social responses in PL-NAc neurons depend on spatial location. To test the hypothesis that the combined social-spatial coding in these neurons contributes to social-spatial learning, we manipulated these neurons during social investigation only in a specific spatial location. Consistent with this hypothesis, these spatially specific manipulations bidirectionally regulated the formation of a preference for the location of the social encounter. These results suggest that the unexpected combination of spatial and social information

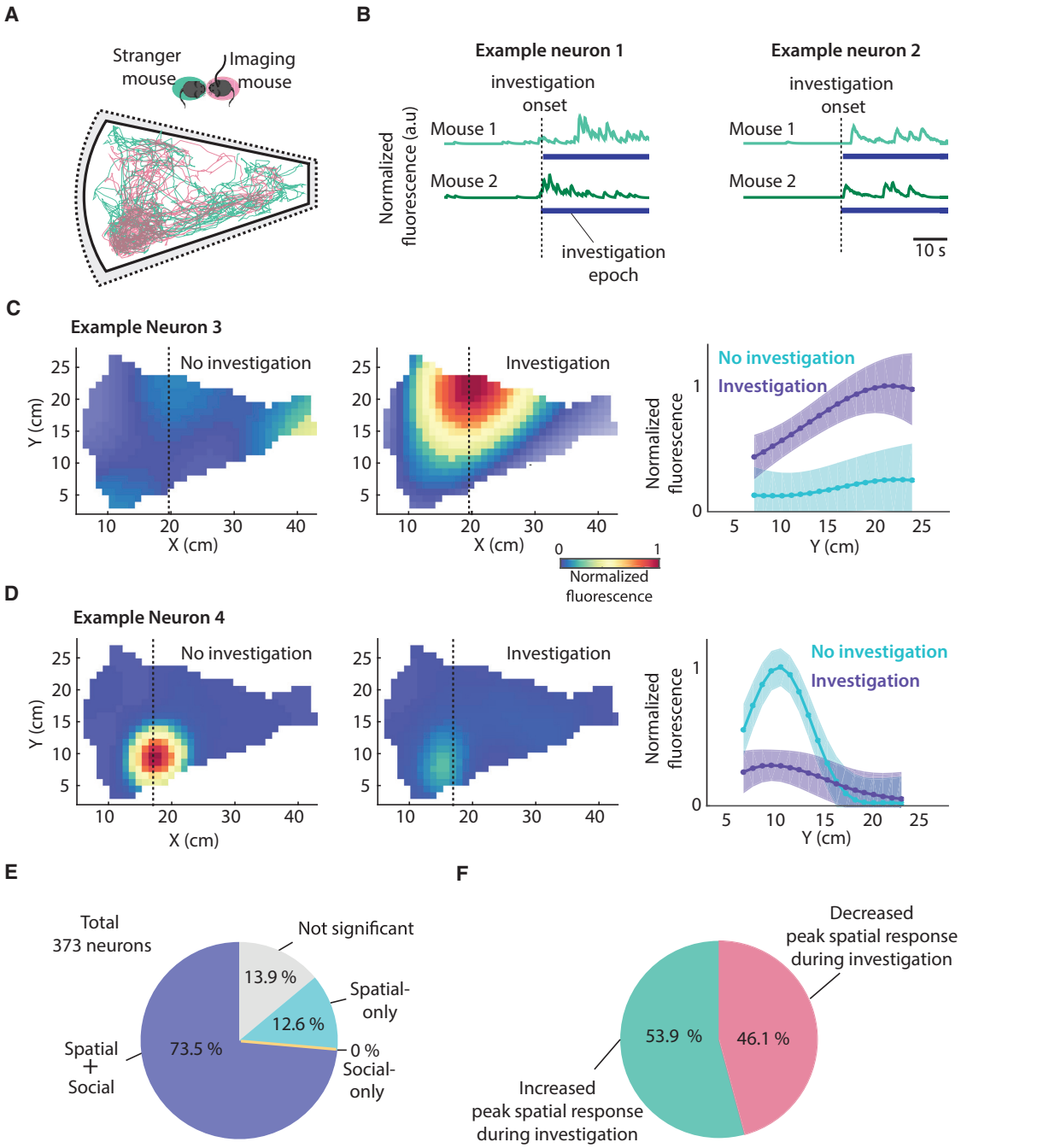

Figure 6. In the Home-Cage Assay, PL-NAc Neurons Respond in a Manner that Depends on Both Social Investigation and Spatial Location

(A) Position tracking data of a representative imaged mouse (pink) and a social target (green) during the home-cage assay. Investigation was defined as epochs when the mouse was engaged in pursuit, sniffing, or grooming of the social target (see the STAR Methods).

(B) Example neurons with elevated activity during social investigation of multiple social targets.

(C) An example neuron with spatial selectivity only during social investigation (middle), but not in the absence of social investigation (left). Right panel: traces of the estimated fluorescence from along a vertical slice (spatial bin with the maximum response) during investigation (purple) and no investigation (aqua).

(D) An example neuron with spatial selectivity only during epochs with no social investigation (left), but not during social investigation (middle). Right panel: traces showing the estimated fluorescence along a vertical slice (spatial bin with the maximum response) during social investigation (purple) and not investigation (aqua). Shaded regions denote error bars (2 SD).

(legend continued on next page)

within the PL-NAc population supports socially motivated behavior by enabling the formation of social-spatial associations. This mechanism may reflect a general contribution of this projection to reward-context learning, even beyond social behavior.

Relevance of a Combined Social-Spatial Code in PL-NAc Neurons

The combined social and spatial code that we observed in PL-NAc neurons could provide a powerful template to support learning to perform appropriate socially motivated behavior in a location-specific manner. In theory, such learning could be mediated by dopamine-dependent synaptic plasticity in the NAc. In this view, PL-NAc synapses that are active during social investigation in a specific spatial location could be strengthened, given the release of dopamine that is known to accompany social investigation (Figure S7C) (Gunaydin et al., 2014). Such plasticity could in turn reinforce conditioned approach behavior to the location of the encounter (i.e., a social-spatial association).

Consistent with this hypothesis, spatially specific inhibition of PL-NAc neurons in the location of a social encounter prevents the formation of a social-spatial association for that location (Figure 7D). This manipulation should preferentially impact PL-NAc neurons that are normally active during social investigation in the inhibited location, and may therefore prevent the synaptic weights of those neurons from changing in the NAc (Figure S7D), while allowing synaptic weights of other neurons to change (e.g., the weights of synapses that are active during investigation of the "control" social target; Figures 7E and S7D). Similarly, spatially specific activation of PL-NAc neurons enhances social-spatial learning, which may enhance synapses that encode the relevant location (Figures 7J and S7E).

Why might spatially uniform activation in the linear 3-chamber assay and home-cage assay have reduced social preference (Figures 2D and 3B), given that spatially specific activation enhanced social spatial learning in the social CPP (Figure 7J)? Spatially uniform activation of PL-NAc neurons is an unnatural pattern of activity. One possibility is that it uniformly strengthens synaptic weights in NAc, regardless of the spatial location that the neurons encode, therefore reducing the relative preference for the location of the social target by effectively increasing preference for other locations (Figure S7F). Consistent with the hypothesis that learning is driving the decrease in social preference from PL-NAc activation in the 3-chamber assay, the change in social preference increased gradually over time during the stimulation epoch (Figure S2J). Similarly, in the post-stimulation epoch, there was a trend toward a sustained reduction in social investigation and increase in novel object investigation (Figures 2D, 2G, and S2H).

An alternative interpretation of our data is that PL-NAc neurons regulate social motivation, rather than social learning. It is difficult to rule out this hypothesis, given that learning and motivation are closely related concepts. However, we believe learning provides a more compelling explanation, given that manipulation of PL-NAc neurons in the social CPP regulates behavior even the day after the manipulation, which implies learning. In addition, in the two assays that were designed to assess social motivation, but not well designed to assess learning (home-cage assay and 3-chamber assay), although activation of PL-NAc neurons decreases social preference, there was no effect from inhibition (similar result in Yizhar et al. [2011]). The lack of effect of inhibition weakens the support for the social motivation hypothesis.

In interpreting the behavior effect of optogenetic inhibition during the social CPP (Figure 7D), we cannot definitively conclude that the effect is being mediated by inhibition of the social-spatial neurons. However, there are a couple reasons to believe this may be the case. First, spatially specific inhibition of PL-NAc neurons in the absence of a social target had no effect on preference (Figures 7F and 7G). Given that this manipulation should inhibit spatial (but not social) responses, this result implies that inhibition of spatial responses alone is not responsible for the behavioral effects observed in the social CPP, and that social responses must contribute. Second, given that social-only neurons compose a small fraction of the observed neurons (~2% in the linear 3-chamber assay and 0% in the home-cage assay), it seems unlikely that social and not social-spatial responses contribute to the behavioral effects in the social CPP.

Conjunctive Codes in Prefrontal Cortex

The combined coding of social and spatial information in PL-NAc neurons is reminiscent of highly conjunctive codes that have been reported in non-human primate prefrontal cortex in decision making tasks (Rigotti et al., 2013; Rainer et al., 1998). It has been suggested that the computational advantage of such "mixed selectivity" is to enable flexible readout of parameters of interest by a linear decoder.

Here, we propose a related function of conjunctive codes. As described in detail above, we propose that a conjunctive code for spatial position and social investigation would provide information about an animal's current state, which is an essential ingredient for reinforcement learning. Thus, a reinforcement learning mechanism could update the value of a spatial location, as represented in NAc, by combining social-spatial information in PL-NAc neurons with a reward prediction error carried by dopamine neurons (Schultz 1998; Hollerman and Schultz, 1998; Eshel et al., 2016; Parker et al., 2016).

Through analogous mechanisms, a conjunctive code in PL-NAc neurons may potentially also support learning about other aspects of social behavior, and other types of reward-location associations. For example, PL-NAc neurons may also respond during consumption of food reward, with different neurons selective for different spatial locations, a coding scheme which could

(E) Of the 373 imaged neurons, 73.5% had responses that were best explained by both social investigation and spatial position, while 12.6% were only spatial and 0% were only social. The remainder were not significantly modulated by either variable. These categories were determined based on comparing cross-validated fits of a social-only model, a spatial-only model, and a spatial+social model on cross-validated data (see the STAR Methods for details).
(F) Of the neurons with response modulation by both social investigation and spatial position (n = 269), 53.9% increased their peak spatial response during social investigation (like in the example neuron in C), whereas 46.1% decreased during investigation (example in D).
See also Figure S6 and Movies S1 and S2.

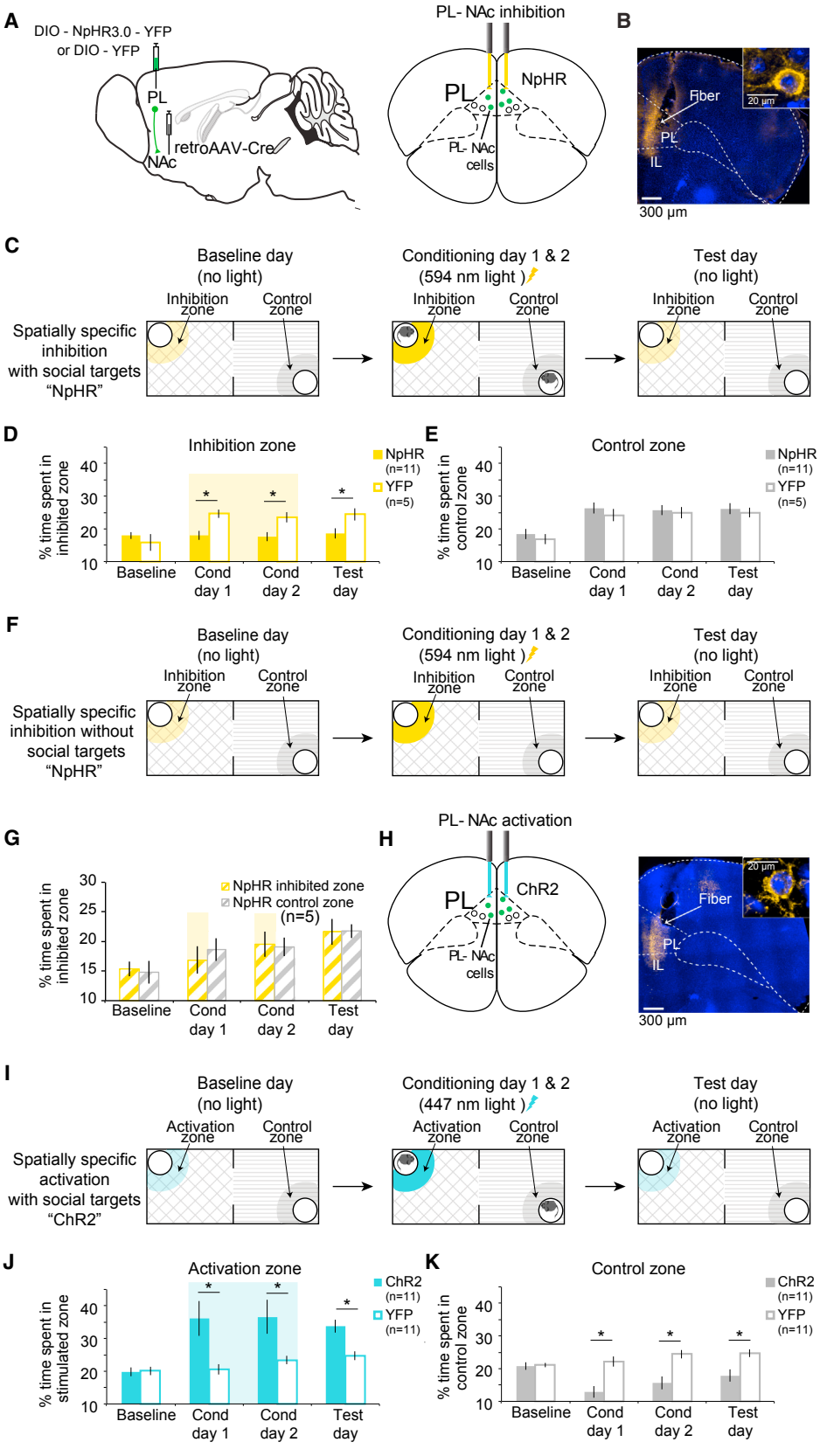

(legend on next page)

potentially support food-context learning. In fact, PL-NAc neurons have been previously implicated in reward-seeking for food and drug reward (Ma et al., 2014; McFarland et al., 2003; Otis et al., 2017; Ye et al., 2016; Land et al., 2014; Britt et al., 2012), although to our knowledge a contribution to the spatial aspect of such behaviors has not been investigated.

Our finding of combined social-spatial coding depended on rigorous analysis of the relationship between neural activity and behavior, which is difficult in the context of social behavior, in part because of the relatively limited amount of time mice spend engaged in social investigation. To overcome this challenge, we employed a Bayesian framework based on Gaussian processes to accurately estimate the relationship between neural activity and behavior (see the STAR Methods).

Connections to Previous Research on Social Behavior and Remaining Open Questions

An important question had been why activation of PL caused mice to spend less time investigating a conspecific, when (spatially non-specific) inhibition of endogenous activity resulted in no observable change in behavior (Yizhar et al., 2011). Here, we demonstrate that in the context of social-spatial learning, inhibition of endogenous activity in PL-NAc neurons does indeed disrupt social behavior. Given that NAc has been implicated in social learning (Okuyama et al., 2016; Dölen et al., 2013; Aragona et al., 2006; Gingrich et al., 2000; Liu and Wang, 2003), and given that social investigation results in dopamine release from the VTA into the NAc (Gunaydin et al., 2014), our results provide a coherent link between previously disparate literatures regarding the involvement of PL, NAc and VTA in social behavior.

A remaining open question is which anatomical inputs provide spatial information to PL-NAc neurons. An obvious candidate is the ventral hippocampus, a region known for its spatial coding, and which projects directly onto PL-NAc neurons (Otis et al., 2017; Spellman et al., 2015). A related question is which inputs provide social information to PL-NAc neurons. Visual, olfactory, somatosensory, and auditory inputs could potentially contribute to the observed neural responses. One possibility is that a reduced social stimulus comprised of only one of those modalities is sufficient to generate social responses in PL-NAc neurons; alternatively, the responses may fundamentally require a multimodal social target. Yet another interesting question is if the responses are better described as sensory or motor. The former would correspond to responses that are better predicted by the behavior of the target mouse, while the latter would correspond to responses that are better predicted by the imaged mouse's behavior. Dissociating between these possibilities may ultimately be possible through detailed measurements and modeling of the behavior of both the imaged as well as the target mouse.

Conclusions

In conclusion, we found that PL-NAc neurons encode a combination of social and spatial information and enable the formation of social-spatial associations. This represents a novel mechanism through which PL may contribute to social behavior, which may generalize to other forms of reward-location learning.

STAR★METHODS

Detailed methods are provided in the online version of this paper and include the following:

- KEY RESOURCES TABLE
- CONTACT FOR REAGENT AND RESOURCE SHARING
- EXPERIMENTAL MODEL AND SUBJECT DETAILS
- METHOD DETAILS
  - Stereotactic surgeries
  - Immunohistochemistry

Figure 7. PL-NAc Neurons Bidirectionally Modulate Social-Spatial Learning

(A) Left: to target NpHR expression to PL-NAc neurons, the retrograde virus retroAAV-Cre was injected in the NAc and Cre-dependent AAV5-DIO-NpHR-YFP or AAV5-DIO-YFP was injected in PL. Right: schematic of fiber placement in PL.

(B) Histology of fiber placement and terminal expression of NpHR-YFP in PL-NAc neurons (YFP expression in yellow and DAPI in blue).

(C) Social conditioned place preference paradigm with spatially specific inhibition. Baseline day: mice explored the 2-chamber arena with empty cages at two ends. Conditioning days (2 days): mice explored the same 2-chamber arena, each with an encaged social target. PL-NAc neurons were inhibited in the proximity of one social target (594 nm, 2.5–3 mW) but not the other. Test day: mice explored the arena in the absence of both social targets and inhibition. Each day the time spent near the cages (social zone) was measured.

(D) In contrast to control mice (YFP, n = 5 animals), mice expressing NpHR (n = 11 animals) in PL-NAc neurons failed to form a preference for the social zone paired with yellow light (conditioning days), and this effect persists the day after (test day) in the absence of any inhibition (ANOVA with group and days as factors; $p = 0.0271$ for group X days, followed by post hoc t test baseline: $p = 0.378$, cond day 1: $p = 0.008$, cond day 2: $p = 0.025$, test day: $p = 0.024$).

(E) Both NpHR and YFP mice acquired a preference for the social zone (control zone) that was not paired with light (ANOVA with group and days as factors; $p = 0.3416$ for group, $p < 0.001$ for days, $p = 0.9851$ for group X days).

(F) The conditioning paradigm was performed like in Figure 7C, but in the absence of any social targets.

(G) In the absence of social targets, inhibition of PL-NAc neurons had no effect on spatial preference (ANOVA with zones and days as factors; $p = 0.775$ for zone X days).

(H) Left: schematic of fiber placement in the PL. PL-NAc neurons targeted based on rAAV-Cre injection in NAc and Cre-dependent AAV5-DIO-ChR2-YFP (or control virus) in PL. Histology of fiber placement and expression of ChR2-YFP in PL-NAc neurons (YFP expression in yellow, DAPI in blue).

(I) Spatially specific activation of PL-NAc neurons in the social CPP. The conditioning paradigm was performed as above (7C), but PL-NAc neurons were activated in the proximity of one social target (447 nm, 1.5 mW, 5-ms long pulses at 10 Hz), but not the other.

(J) Mice expressing ChR2 (n = 11 animals) in PL-NAc neurons acquired a stronger preference relative to the control mice (YFP, n = 11 animals) for the social zone paired with blue light (conditioning days), and this effect persists the day after (test day), in the absence of any activation (ANOVA with group and days as factors; $p = 0.043$ for group X days, followed by post hoc t tests for baseline: $p = 0.897$, cond day 1: $p = 0.011$, cond day 2: $p = 0.021$, test day: $p = 0.001$).

(K) ChR2 mice spent less time in the social zone that was not paired with light relative to the YFP mice (ANOVA with group and days as factors; $p = 0.012$ for group X days, followed by post hoc t test for baseline: $p = 0.805$, cond day 1: $p = 0.0008$, cond day 2: $p = 0.001$, test day: $p = 0.005$).

Data are presented as mean ± SEM. See also Figure S7.

SUPPLEMENTAL INFORMATION

Supplemental Information includes seven figures, one table, and two movies and can be found with this article online at https://doi.org/10.1016/j.cell.2017.11.002.

AUTHOR CONTRIBUTIONS

Conceptualization, M.M. and I.B.W.; Methodology, A.R.N. and M.M.; Formal Analysis, J.W.P., H.H., Y.L., and M.M.; Investigation, M.M., H.J.J., M.P., E.M.M., J.C., J.P.T., N.F.P., V.B., A.R.N. and I.B.W.; Writing–Original Draft, M.M. and I.B.W.; Writing–Review & Editing, M.M. and I.B.W.; Funding Acquisition, M.M. and I.B.W.; Supervision, M.M., A.R.N., and I.B.W.

ACKNOWLEDGMENTS

We thank B. Engelhard, S. Bolkan, and the rest of the Witten lab for comments and advice on this work; E. Kremer and E. Engel for reagents; and B. Patel for technical assistance. This work was funded by Pew, McKnight, and Sloan Foundation grants to I.B.W., the NIH (DP2 DA035149-01 and 5R01MH106689-02 to I.B.W. and 1F32MH112320-01A1 to J.C.), SCGB (412733 to M.M.), NSF GRFP (to N.F.P.), NARSAD Young Investigator Awards (to A.R.N. and I.B.W.), and NCATS NIH CTSA program (UL1 TR001866 to Y.L. and H.H.). I.B.W. is a New York Stem Cell Foundation—Robertson Investigator. J.W.P. was supported by grants from the McKnight Foundation, Simons Collaboration on the Global Brain (SCGB AWD1004351), and the NSF CAREER Award (IIS-1150186).

Received: March 28, 2017
Revised: September 3, 2017
Accepted: October 31, 2017
Published: December 7, 2017

REFERENCES

Amadei, E.A., Johnson, Z.V., Jun Kwon, Y., Shpiner, A.C., Saravanan, V., Mays, W.D., Ryan, S.J., Walum, H., Rainnie, D.G., Young, L.J., and Liu, R.C. (2017). Dynamic corticostriatal activity biases social bonding in monogamous female prairie voles. Nature *546*, 297–301.

Aragona, B.J., Liu, Y., Yu, Y.J., Curtis, J.T., Detwiler, J.M., Insel, T.R., and Wang, Z. (2006). Nucleus accumbens dopamine differentially mediates the formation and maintenance of monogamous pair bonds. Nat. Neurosci. *9*, 133–139.

Berendse, H.W., Galis-de Graaf, Y., and Groenewegen, H.J. (1992). Topographical organization and relationship with ventral striatal compartments of prefrontal corticostriatal projections in the rat. J. Comp. Neurol. *316*, 314–347.

Bicks, L.K., Koike, H., Akbarian, S., and Morishita, H. (2015). Prefrontal cortex and social cognition in mouse and man. Front. Psychol. *6*, 1805.

Bishop, C.M. (2006). Pattern Recognition and Machine Learning (Springer).

Britt, J.P., Benaliouad, F., McDevitt, R.A., Stuber, G.D., Wise, R.A., and Bonci, A. (2012). Synaptic and behavioral profile of multiple glutamatergic inputs to the nucleus accumbens. Neuron *76*, 790–803.

Carr, D.B., and Sesack, S.R. (2000). Projections from the rat prefrontal cortex to the ventral tegmental area: target specificity in the synaptic associations with mesoaccumbens and mesocortical neurons. J. Neurosci. *20*, 3864–3873.

Dölen, G., Darvishzadeh, A., Huang, K.W., and Malenka, R.C. (2013). Social reward requires coordinated activity of nucleus accumbens oxytocin and serotonin. Nature *501*, 179–184.

Ekstrand, M.I., Nectow, A.R., Knight, Z.A., Latcha, K.N., Pomeranz, L.E., and Friedman, J.M. (2014). Molecular profiling of neurons based on connectivity. Cell *157*, 1230–1242.

Eshel, N., Tian, J., Bukwich, M., and Uchida, N. (2016). Dopamine neurons share common response function for reward prediction error. Nat. Neurosci. *19*, 479–486.

Felix-Ortiz, A.C., Burgos-Robles, A., Bhagat, N.D., Leppla, C.A., and Tye, K.M. (2016). Bidirectional modulation of anxiety-related and social behaviors by amygdala projections to the medial prefrontal cortex. Neuroscience *321*, 197–209.

Friard, O., and Gamba, M. (2016). BORIS: a free, versatile open-source event-logging software for video/audio coding and live observations. Methods Ecol. Evol. *7*, 1325–1330.

Ghosh, K.K., Burns, L.D., Cocker, E.D., Nimmerjahn, A., Ziv, Y., Gamal, A.E., and Schnitzer, M.J. (2011). Miniaturized integration of a fluorescence microscope. Nat. Methods *8*, 871–878.

Gingrich, B., Liu, Y., Cascio, C., Wang, Z., and Insel, T.R. (2000). Dopamine D2 receptors in the nucleus accumbens are important for social attachment in female prairie voles (Microtus ochrogaster). Behav. Neurosci. *114*, 173–183.

Gunaydin, L.A., Grosenick, L., Finkelstein, J.C., Kauvar, I.V., Fenno, L.E., Adhikari, A., Lammel, S., Mirzabekov, J.J., Airan, R.D., Zalocusky, K.A., et al. (2014). Natural neural projection dynamics underlying social behavior. Cell *157*, 1535–1551.

Heidbreder, C.A., and Groenewegen, H.J. (2003). The medial prefrontal cortex in the rat: evidence for a dorso-ventral distinction based upon functional and anatomical characteristics. Neurosci. Biobehav. Rev. *27*, 555–579.

Hitti, F.L., and Siegelbaum, S.A. (2014). The hippocampal CA2 region is essential for social memory. Nature *508*, 88–92.

Hollerman, J.R., and Schultz, W. (1998). Dopamine neurons report an error in the temporal prediction of reward during learning. Nat. Neurosci. *1*, 304–309.

Kabra, M., Robie, A.A., Rivera-Alba, M., Branson, S., and Branson, K. (2013). JAABA: interactive machine learning for automatic annotation of animal behavior. Nat. Methods *10*, 64–67.

Kim, C.K., Ye, L., Jennings, J.H., Pichamoorthy, N., Tang, D.D., Yoo, A.W., Ramakrishnan, C., and Deisseroth, K. (2017). Molecular and circuit-dynamical identification of top-down neural mechanisms for restraint of reward seeking. Cell *170*, 1013–1027.e14.

Land, B.B., Narayanan, N.S., Liu, R.J., Gianessi, C.A., Brayton, C.E., Grimaldi, D.M., Sarhan, M., Guarnieri, D.J., Deisseroth, K., Aghajanian, G.K., and DiLeone, R.J. (2014). Medial prefrontal D1 dopamine neurons control food intake. Nat. Neurosci. *17*, 248–253.

Lee, E., Rhim, I., Lee, J.W., Ghim, J.W., Lee, S., Kim, E., and Jung, M.W. (2016a). Enhanced neuronal activity in the medial prefrontal cortex during social approach behavior. J. Neurosci. *36*, 6926–6936.

Lee, J., Finkelstein, J., Choi, J.Y., and Witten, I.B. (2016b). Linking cholinergic interneurons, synaptic plasticity, and behavior during the extinction of a cocaine-context association. Neuron *90*, 1071–1085.

Lein, E.S., Hawrylycz, M.J., Ao, N., Ayres, M., Bensinger, A., Bernard, A., Boe, A.F., Boguski, M.S., Brockway, K.S., Byrnes, E.J., et al. (2007). Genome-wide atlas of gene expression in the adult mouse brain. Nature *445*, 168–176.

Lin, D., Boyle, M.P., Dollar, P., Lee, H., Lein, E.S., Perona, P., and Anderson, D.J. (2011). Functional identification of an aggression locus in the mouse hypothalamus. Nature *470*, 221–226.

Liu, Y., and Wang, Z.X. (2003). Nucleus accumbens oxytocin and dopamine interact to regulate pair bond formation in female prairie voles. Neuroscience *121*, 537–544.

Ma, Y.-Y., Lee, B.R., Wang, X., Guo, C., Liu, L., Cui, R., Lan, Y., Balcita-Pedicino, J.J., Wolf, M.E., Sesack, S.R., et al. (2014). Bidirectional modulation of incubation of cocaine craving by silent synapse-based remodeling of prefrontal cortex to accumbens projections. Neuron *83*, 1453–1467.

McFarland, K., Lapish, C.C., and Kalivas, P.W. (2003). Prefrontal glutamate release into the core of the nucleus accumbens mediates cocaine-induced reinstatement of drug-seeking behavior. J. Neurosci. *23*, 3531–3537.

Nectow, A.R., Ekstrand, M.I., and Friedman, J.M. (2015). Molecular characterization of neuronal cell types based on patterns of projection with Retro-TRAP. Nat. Protoc. *10*, 1319–1327.

Nectow, A.R., Schneeberger, M., Zhang, H., Field, B.C., Renier, N., Azevedo, E., Patel, B., Liang, Y., Mitra, S., Tessier-Lavigne, M., et al. (2017a). Identification of a brainstem circuit controlling feeding. Cell *170*, 429–442.e11.

Nectow, A.R., Moya, M.V., Ekstrand, M.I., Mousa, A., McGuire, K.L., Sferrazza, C.E., Field, B.C., Rabinowitz, G.S., Sawicka, K., Liang, Y., et al. (2017b). Rapid molecular profiling of defined cell types using viral TRAP. Cell Rep. *19*, 655–667.

Okuyama, T., Kitamura, T., Roy, D.S., Itohara, S., and Tonegawa, S. (2016). Ventral CA1 neurons store social memory. Science *353*, 1536–1541.

Otchy, T.M., Wolff, S.B., Rhee, J.Y., Pehlevan, C., Kawai, R., Kempf, A., Gobes, S.M., and Ölveczky, B.P. (2015). Acute off-target effects of neural circuit manipulations. Nature *528*, 358–363.

Otis, J.M., Namboodiri, V.M., Matan, A.M., Voets, E.S., Mohorn, E.P., Kosyk, O., McHenry, J.A., Robinson, J.E., Resendez, S.L., Rossi, M.A., and Stuber, G.D. (2017). Prefrontal cortex output circuits guide reward seeking through divergent cue encoding. Nature *543*, 103–107.

Panksepp, J.B., and Lahvis, G.P. (2007). Social reward among juvenile mice. Genes Brain Behav. *6*, 661–671.

Park, M., Weller, J.P., Horwitz, G.D., and Pillow, J.W. (2014). Bayesian active learning of neural firing rate maps with transformed gaussian process priors. Neural Comput. *26*, 1519–1541.

Parker, N.F., Cameron, C.M., Taliaferro, J.P., Lee, J., Choi, J.Y., Davidson, T.J., Daw, N.D., and Witten, I.B. (2016). Reward and choice encoding in terminals of midbrain dopamine neurons depends on striatal target. Nat. Neurosci. *19*, 845–854.

Pascoli, V., Terrier, J., Espallergues, J., Valjent, E., O'Connor, E.C., and Lüscher, C. (2014). Contrasting forms of cocaine-evoked plasticity control components of relapse. Nature *509*, 459–464.

Paxinos, G., and Franklin, K.B.J. (2004). The Mouse Brain in Stereotaxic Coordinates (Gulf Professional Publishing).

Pearson, B.L., Bettis, J.K., Meyza, K.Z., Yamamoto, L.Y., Blanchard, D.C., and Blanchard, R.J. (2012). Absence of social conditioned place preference in BTBR T+tf/J mice: relevance for social motivation testing in rodent models of autism. Behav. Brain Res. *233*, 99–104.

Rainer, G., Asaad, W.F., and Miller, E.K. (1998). Memory fields of neurons in the primate prefrontal cortex. Proc. Natl. Acad. Sci. USA *95*, 15008–15013.

Rigotti, M., Barak, O., Warden, M.R., Wang, X.J., Daw, N.D., Miller, E.K., and Fusi, S. (2013). The importance of mixed selectivity in complex cognitive tasks. Nature *497*, 585–590.

Ritchie, M.E., Phipson, B., Wu, D., Hu, Y., Law, C.W., Shi, W., and Smyth, G.K. (2015). limma powers differential expression analyses for RNA-sequencing and microarray studies. Nucleic Acids Res. *43*, e47.

Robinson, M.D., McCarthy, D.J., and Smyth, G.K. (2010). edgeR: a Bioconductor package for differential expression analysis of digital gene expression data. Bioinformatics *26*, 139–140.

Schultz, W. (1998). Predictive reward signal of dopamine neurons. J. Neurophysiol. *80*, 1–27.

Spellman, T., Rigotti, M., Ahmari, S.E., Fusi, S., Gogos, J.A., and Gordon, J.A. (2015). Hippocampal-prefrontal input supports spatial encoding in working memory. Nature *522*, 309–314.

Takahashi, A., Nagayasu, K., Nishitani, N., Kaneko, S., and Koide, T. (2014). Control of intermale aggression by medial prefrontal cortex activation in the mouse. PLoS ONE *9*, e94657.

Tervo, D.G.R., Hwang, B.Y., Viswanathan, S., Gaj, T., Lavzin, M., Ritola, K.D., Lindo, S., Michael, S., Kuleshova, E., Ojala, D., et al. (2016). A designer AAV variant permits efficient retrograde access to projection neurons. Neuron *92*, 372–382.

van Kerkhof, L.W., Damsteegt, R., Trezza, V., Voorn, P., and Vanderschuren, L.J. (2013). Social play behavior in adolescent rats is mediated by functional activity in medial prefrontal cortex and striatum. Neuropsychopharmacology *38*, 1899–1909.

Wang, F., Zhu, J., Zhu, H., Zhang, Q., Lin, Z., and Hu, H. (2011). Bidirectional control of social hierarchy by synaptic efficacy in medial prefrontal cortex. Science *334*, 693–697.

Wong, L.C., Wang, L., D'Amour, J.A., Yumita, T., Chen, G., Yamaguchi, T., Chang, B.C., Bernstein, H., You, X., Feng, J.E., et al. (2016). Effective modulation of male aggression through lateral septum to medial hypothalamus projection. Curr. Biol. *26*, 593–604.

Ye, L., Allen, W.E., Thompson, K.R., Tian, Q., Hsueh, B., Ramakrishnan, C., Wang, A.C., Jennings, J.H., Adhikari, A., Halpern, C.H., et al. (2016). Wiring and molecular features of prefrontal ensembles representing distinct experiences. Cell *165*, 1776–1788.

Yizhar, O., Fenno, L.E., Prigge, M., Schneider, F., Davidson, T.J., O'Shea, D.J., Sohal, V.S., Goshen, I., Finkelstein, J., Paz, J.T., et al. (2011). Neocortical excitation/inhibition balance in information processing and social dysfunction. Nature *477*, 171–178.

Zhou, P., Resendez, S.L., Rodriguez-Romaguera, J., Jimenez, J.C., Neufeld, S.Q., Stuber, G.D., Hen, R., Kheirbek, M.A., Sabatini, B.L., Kass, R.E., et al. (2016). Efficient and accurate extraction of in vivo calcium signals from microendoscopic video data. arXiv, arXiv:1605.07266, https://arxiv.org/abs/1605.07266.

STAR★METHODS

KEY RESOURCES TABLE

REAGENT or RESOURCE	SOURCE	IDENTIFIER
Antibodies		
Mouse monoclonal anti-GFP	Life Technologies Corporation	G10362
Donkey anti-rabbit coupled to Alexa 488	Jackson ImmunoResearch	711-545-152
Bacterial and Virus Strains		
AAV 2/5-IV-GFPL10	Nectow et al., 2017a PNI Viral Core, Princeton	https://www.addgene.org/98704/
CAV-Cre virus	IGMM Vector core, France	N/A
AAV 2/5-CAG-Flex-GCamp6f-WPRE-SV40	UPenn Vector Core	AV-5-PV2816
AAV 2/5-CamKIIa-hChR2-EYFP	UNC Vector Core	https://www.addgene.org/26969/
AAV 2/5-CamKIIa-EYFP	UNC Vector Core	http://www.everyvector.com/sequences/show_public/11037
retro AAV-Ef1a-NLS-Cre_WPRE-hGHpA	Tervo et al., 2016 PNI Viral Core, Princeton	https://www.addgene.org/55636/
AAV 2/5-EF1a-DIO-NpHR3.0-EYFP	UPenn Vector Core	https://www.addgene.org/26966/
AAV 2/5-EF1a-DIO-YFP	UPenn Vector Core	https://www.addgene.org/27056/
AAV 2/5-EF1a-DIO-ChR2-EYFP	PNI Vector Core	http://www.everyvector.com/sequences/show_public/2491
Chemicals, Peptides, and Recombinant Proteins		
CTB-488	Life Technologies Corporation	C22841
CTB-555	Life Technologies Corporation	C22843
CTB-647	Life Technologies Corporation	C34778
Critical Commercial Assays		
RNAscope Multiplex Fluorescent Assay	Advanced Cell Diagnostics, Inc.	323110
TSA Plus Cyanine 3 in C2 and TSA Plus Cyanine 5 in C3	Perkin Elmer	NEL760001KT
Deposited Data		
RNA sequencing data for PL-NAc, PL-Amyg and PL-VTA projections	Data generated by this study.	GEO: GSE104943; https://www.ncbi.nlm.nih.gov/geo/query/acc.cgi
Experimental Models: Organisms/Strains		
Mouse: wild type C57BL/6J	Jackson Laboratory	JAX: 000664
Software and Algorithms		
Spatial estimation using GP regression	Generated by this study	https://github.com/wittenlab/Spatial-field-estimates-Murugan-et-al-Cell-2017#gp-regression-for-place-field-estimation
JABBA	Janelia	N/A
BORIS	Friard and Gamba, 2016	http://www.boris.unito.it
AfterEffects	Adobe	N/A
Other		
Fibers for optogenetics	Thor Labs	BFL37-300
Ferrules for optogenetics	Precision Fiber Products	MM-FER-2006SS- 3300
0.5 mm diameter, ~6.1 mm length GRIN lens	Inscopix	GLP-0561
1 mm diameter, ~4.3 mm length Prism probes	Inscopix	PPL-1043
Imaging Baseplate	Inscopix	BPL-2
Baseplate cover	Inscopix	BPC-2

CONTACT FOR REAGENT AND RESOURCE SHARING

Further information and requests for resources and reagents should be directed to and will be fulfilled by the Lead Contact, Ilana Witten (iwitten@princeton.edu).

EXPERIMENTAL MODEL AND SUBJECT DETAILS

All experimental procedures were conducted in accordance with the National Institutes of Health guidelines and were reviewed by the Princeton University Institutional Animal Care and Use Committee (IACUC). For all experiments, male and female C57BL/6J mice aged 6-10 weeks from The Jackson Laboratory (strain 000664) were used. Mice were maintained on a 12-hour light on – 12-hour light off schedule. All surgical manipulations and behavioral tests were conducted during their light off period.

METHOD DETAILS

Stereotactic surgeries

Mice were anaesthetized with 1%–2% isoflurane and placed in a stereotactic setup. A microsyringe was used to deliver virus or neural tracer to target brain regions.

For retrograde tracing experiments (Figures 1A–1F, S1A, and S1B), 0.3 – 0.5 μL of cholera toxin β subunit conjugated to fluorophores (CTB-488, CTB-555, CTB-647, Life Technologies Corporation) was injected unilaterally into the NAc core (1.3 mm anterior, 1.0 mm lateral and 4.7 mm in depth, n = 6 animals), VTA (3.3 mm posterior, 0.7 mm lateral and 4.7 mm depth, n = 7 animals) and/or amygdala (1.6 mm posterior, 2.8 mm lateral and 4.8 mm depth, n = 5 animals) of mice aged 6-10 weeks.

For molecular profiling experiments (Figures 1G, 1H, S1C, and S1D), to specifically target PL projection subpopulations, mice aged ~8 weeks were bilaterally injected in the PL (1.8 mm anterior, 0.5 mm lateral and 2.5 mm in depth) with 1 μL of AAV5-IV-GFPL10 and 0.75 μL of a retrogradely transporting CAV-Cre virus (IGMM Vector core, France, ~2.5 × 10^{12} parts/ml) into the Amyg, NAc or VTA.

For the fluorescence *in situ* hybridization experiments (Figure 1I), for each projection, 750 nL of CAV-Cre virus (IGMM Vector core, France, ~2.5 × 10^{12} parts/ml) was injected in the NAc (1.2 mm anterior, 1.1 mm lateral and 4.7 mm in depth), BLA (1.4 mm posterior, 3.6 mm lateral and 4.9 mm in depth), or VTA (3.0 mm posterior, 0.5 mm lateral, and 4.7 mm in depth) and 750 nL of AAV5-CAG-Flex-GCaMP6f-WPRE-SV40 virus (UPenn Vector Core, injected titer of 3.53 × 10^{12} parts/ml) was injected into the PL (1.8 mm anterior, 0.5 mm lateral and 2.5 mm in depth) of mice aged 6 weeks.

For PL terminal activation experiments (Figures 2, 3, S2, S3A, and S3B), mice aged ~6 weeks were bilaterally injected in the PL (1.8 mm anterior, 0.5 mm lateral and 2.5 mm in depth) with 1 μL of AAV5-CaMKIIa-hChR2-EYFP (n = 35 ChR2 mice, UNC Vector Core, 4 × 10^{12} parts/ml and 8 × 10^{12} parts/ml) or AAV5-CaMKIIa-EYFP (n = 30 control mice, UNC Vector Core, final titer of 7.5 × 10^{12} parts/ml) virus. Ferrules attached to optical fibers (300 μm core diameter, 0.37 NA) were implanted bilaterally to target either the NAc core (1.3 mm anterior, 1.0 mm lateral and 4.3 mm in depth, ChR2 n = 13, YFP n = 11 animals, Home-cage assay, ChR2, YFP n = 8 n = 10), Amyg (1.6 mm posterior, 3.4 mm lateral and 4.3 mm in depth, ChR2 n = 11, YFP n = 11 animals) or the VTA (3.3 mm posterior, 0.7 mm lateral and 4.3 mm depth, ChR2 n = 11, YFP n = 8 animals).

For imaging experiments (Figures 4, 5, 6, S4, S5, and S6), to specifically target PL neurons projecting to the NAc, mice aged ~8 weeks (n = 16 animals) were injected with 0.75 μL of a retrogradely transporting CAV-Cre virus (IGMM Vector core, France, ~2.5 × 10^{12} parts/ml) into the NAc (1.3 mm anterior, 1.0 mm lateral and 4.7 mm in depth) and 0.75 μL of AAV5-CAG-Flex-GCaMP6f-WPRE-SV40 (UPenn Vector Core, injected titer of 3.53 × 10^{12} parts/ml) into the PL (1.8 mm anterior, 0.5 mm lateral and 2.5 mm in depth). A week post injection, mice were implanted with a 0.5 mm diameter, ~6.1 mm length GRIN lens (GLP-0561, Inscopix) or a 1 mm diameter, ~4.3 mm length Prism probes (PPL-1043, Inscopix) over the PL (1.8 mm anterior, 0.3 mm lateral and 1.9-2.0 mm in depth). A plastic cap was glued to protect the lens. Mice were housed individually post lens implant. 3-4 weeks after the injection, a baseplate (BPL-2, Inscopix) attached to the miniature microscope (nVISTA HD v2, Inscopix) was positioned over the GRIN lens such that the neurons and/or other structures (such as blood vessels) in the brain were in focus. The baseplate was then implanted using dental cement, and a baseplate cover (BPC-2, Inscopix) protected the GRIN lens.

For PL-NAc cell body inhibition experiments (Figures 7A–7G, S3C–S3F, S7A, and S7B), to specifically target PL neurons projecting to the NAc, mice aged ~6 weeks (NpHR: n = 12 animals, YFP: n = 5 animals) were injected with 0.75 μL of a retrogradely transporting retroAAV-Cre virus (Tervo et al., 2016) (PNI Viral core, 1.16 × 10^{14} parts/ml) into the NAc (1.3 mm anterior, 1.0 mm lateral and 4.7 mm in depth) and 0.5 μL of AAV5-EF1a-DIO-NpHR3.0-EYFP (UPenn Vector Core, injected titer of 1.29x10^{13} parts/ml) or AAV5-EF1a-DIO-YFP (UPenn Vector Core, 8.41x10^{12} parts/ml) into the PL (1.8 mm anterior, 0.5 mm lateral and 2.5 mm in depth). Ferrules attached to optical fibers (300 μm core diameter, 0.37 NA) were implanted bilaterally to target the PL.

For PL-NAc cell body activation experiments (Figures 7H–7K), to specifically target PL neurons projecting to the NAc, mice aged ~6 weeks (ChR2: n = 11 animals, YFP: n = 11 animals) were injected with 0.75 μL of a retrogradely transporting retroAAV-Cre virus (PNI Viral core, 1.16 × 10^{14} parts/ml) into the NAc (1.3 mm anterior, 1.0 mm lateral and 4.7 mm in depth) and 0.5 μL of AAV5-EF1a-DIO-ChR2-EYFP (PNI Vector Core, injected titer of 1.4x10^{14} parts/ml) or AAV5-EF1a-DIO-YFP (UPenn Vector Core, 8.41x10^{12} parts/ml) into the PL (1.8 mm anterior, 0.5 mm lateral and 2.5 mm in depth). Ferrules attached to optical fibers (300 μm core diameter, 0.37 NA) were implanted bilaterally to target the PL.

Immunohistochemistry

Mice were anesthetized with 0.08 mL Euthasol (i.p. injection) and transcardially perfused with 1x phosphate-buffered saline (PBS), followed by fixation with 4% paraformaldehyde in PBS (PFA). Brains were dissected out and post-fixed in 4% PFA overnight before being transferred into 30% sucrose in PBS solution. 40 μm thick coronal sections containing the brain region of interest were cut on a freezing microtome.

For the retrograde tracing experiments (Figures 1A–1F, S1A, and S1B), we first verified that the CTB injections were localized to the target brain regions (NAc, VTA and the Amyg). Coronal sections containing the PL were then imaged (Nikon Ti2000E) in order to confirm retrograde labeling of NAc-projecting, Amyg-projecting, and/or VTA-projecting neurons in PL. Using Paxinos and Franklin (2004) as a reference, for each animal three CTB-labeled brain sections were chosen along the anterior-posterior axis (~1.5 mm, ~2.2 mm, and ~2.6 mm anterior to bregma). Cellular resolution images of coronal sections of interest were then acquired through the 63x immersion objective using the Leica TCS SP8 confocal microscope. The boundary of prelimbic cortex was determined using measurements from a mouse brain atlas (Paxinos and Franklin, 2004), and all CTB-labeled cells within PL were assessed. The extent of co-labeling and the distance from the midline were measured for each cell using tools in the Leica imaging software suite. For the data presented in Figure 1E, the M/L cell distributions were averaged at 3 anterior-posterior locations (1.5 mm, 2.2 mm and 2.6 anterior to bregma, for separate M /L cell distributions at 3 A/P locations see Figure S1B). 12/30 mice were excluded from the CTB experiments because of failed injection or for not showing any CTB expression.

For the Fluorescent *In Situ* Hybridization experiments (FISH; Figure 1I), 3 weeks after the injections, mice were anesthetized with 0.1 mL Euthasol (i.p. injection) and transcardially perfused with 1x phosphate-buffered saline (PBS), followed by fixation with 4% paraformaldehyde (PFA) in PBS. Brains were dissected out and post-fixed in 4% PFA overnight. Brains were then put through a sucrose gradient: 10% sucrose in PBS solution for 6-8 hours, 20% sucrose in PBS solution overnight, and then 30% sucrose in PBS solution overnight. 18 μm thick coronal sections containing the prelimbic cortex were cut on a cryostat. *In situ* hybridization was performed on mounted sections using the RNAscope Multiplex Fluorescent Assay (Advanced Cell Diagnostics, Inc., No. 323110). Custom probes were used for Pou3f1 (Mm-Pou3f1-C2, 1:50 dilution) and Tnnc1 (Mm-Tnnc1-C3, 1:50 dilution) and diluted in probe diluent provided in the RNAscope kit. Fluorophores used were TSA Plus Cyanine 3 in C2 and TSA Plus Cyanine 5 in C3 (Perkin Elmer, No. NEL760001KT). Fluorophores were reconstituted in 60 μL DMSO and diluted in TSA buffer provided in the RNAscope kit at a concentration of 1:800. Following the *in situ* hybridization protocol, a GFP antibody stain was used to enhance visualization of GCaMP expression. The primary antibody was a mouse monoclonal anti-GFP (1:1000 dilution, Life Technologies, No. G10362) and the secondary was a donkey anti-rabbit coupled to Alexa 488 (1:1000 dilution, Jackson ImmunoResearch, No. 711-545-152). Cellular resolution images of mounted coronal sections were acquired through the 63x immersion objective using the Leica TCS SP8 confocal microscope. The boundary of prelimbic cortex was determined using measurements from a mouse brain atlas (Paxinos and Franklin, 2004). 3/6 mice were excluded for showing no GCaMP6f expression.

For PL terminal activation experiments (Figures 2A, 2B, S2A, and S3A), a GFP antibody stain was used to enhance visualization of virus expression in terminals. The primary antibody was a mouse monoclonal anti-GFP (1:1000, Life Technologies, No. G10362) and the secondary was a donkey anti-rabbit coupled to Alexa 488 (1:1000 dilution, Jackson ImmunoResearch, No. 711-545-152). Mounted sections were imaged to confirm expression of the virus in PL cell bodies and terminals in the NAc, VTA and the Amyg and optical fiber targeting in the downstream structures. 9/74 mice were excluded from the optogenetic studies: 2 mice for seizing during stimulation, 6 mice for failed fiber targeting and 1 mouse for technical problems encountered during behavioral testing.

For the GCaMP6f imaging experiments (Figures 4B and S4A, coronal sections of PL were used to confirm virus expression, nuclear exclusion of GCaMP6f, and to verify targeting of the GRIN lens to PL. 5/21 mice were excluded from the imaging experiments: 1 mouse for the GRIN lens implant being too posterior and 4 mice for showing no GCaMP6f expression.

For PL-NAc cell body optogenetic inhibition (Figures 7B and S7A) and activation experiments (Figure 7H), coronal sections of PL were used to confirm virus expression, nuclear exclusion of NpHR/ChR2, and to verify targeting of the fibers to PL.

Molecular profiling experiment

For molecular profiling experiments (Figures 1G, 1H, S1C, and S1D), approximately 5 weeks post-injection, mice were sacrificed and their brains were rapidly dissected on ice to isolate medial prefrontal cortex. The dissected brain tissue from 6 mice were combined to form a single sample (number of samples- Amyg: 3, NAc: 3, VTA: 2). As described previously (Ekstrand et al., 2014; Nectow et al., 2015, 2017a, 2017b), GFPL10-positive ribosomes were then immunoprecipitated using a 2 hr GFP immunoprecipitation (GFP IP). qPCR analysis was performed using TaqMan assays for the targeted genes to determine differential enrichment (Figure S1C). Fold-enrichment was calculated as IP RNA/Total RNA. Sixteen samples were sequenced (8 IPs paired with 8 Inputs) using 100 bp single reads on an Illumina HiSeq 2500 and evaluated using FASTQC. Reads were then aligned to the mouse reference genome (version mm10) through STAR (https://www.ncbi.nlm.nih.gov/pubmed/23104886). Aligned reads were then summarized through featureCounts (https://www.ncbi.nlm.nih.gov/pubmed/24227677) with the gene model from Ensemble (Mus_musculus.GRCm38.75.gtf) at gene level edgeR (Robinson et al., 2010) was used to normalize counts across samples, and voom (Ritchie et al., 2015) was applied to the normalized counts to estimate the fold change (IP/Input).

In vivo electrophysiology experiment

For electrophysiology experiments (Figures S2B–S2F), ~15 weeks post injection of ChR2 in PL, mice were anaesthetized with urethane (1.2 mg/g). A ~125 μ m tungsten electrode (A-M systems) was glued to a fiber optic (300 μm core diameter, Thor labs) to make an optrode. The optrode was then lowered to the recording sites using stereotactic coordinates (PL:1.8 mm anterior, 0.5 mm lateral and 2.5 mm in depth, NAc: 1.3 mm anterior, 1.0 mm lateral and 4.3 mm in depth, Amyg:1.6 mm posterior, 3.4 mm lateral and 4.3 mm in depth or the VTA:3.3 mm posterior, 0.7 mm lateral and 4.3 mm depth). Spike 2 (CED) was used for data acquisition. To verify ChR2 expression in PL and its terminals in NAc, VTA and Amyg, light pulses of 2 s (447nm, 5 mW at the tip of the optical fiber) were delivered at regular intervals (every 15 s) for many trials (30-50). Spike 2 in combination with custom MATLAB software was used for analyzing the data. A paired t test comparing firing rates of individual neurons before and during light stimulation was used to determine if a neuron was significantly modulated by light stimulation.

Behavior Assays

Linear 3-chamber assay

In this assay, mice explored a linear three-chamber arena with distinct textured floors containing an encaged stranger mouse (juvenile males < than 6 weeks, adult males > 8 weeks or adult estrous females > 8 weeks old) in one side-chamber (the "social target") and an encaged novel object on the other side-chamber. The novel object used in our study were plastic toys (unless stated otherwise) roughly 7x3.5x5 cm in dimension (Figure S2G). Ethovision (Noldus) was used to track the location of the mouse for all linear 3-chamber assays.

For PL terminal activation experiments (Figures 2 and S2), ~14 weeks after injection of ChR2/YFP virus in PL, mice were run on the linear 3-chamber assay. Juvenile male mice were used as social targets for these experiments. The experimenter was blind to the treatment group during the course of the assay. The mice were allowed to explore the linear chamber for 3 min with no light stimulation, followed by 3 min of blue light stimulation (447nm, ~7 mW at the tip of the optical fiber; 5 ms long pulses at 20Hz) and terminating with an additional 3 min of no light. The location of the mice was tracked using Ethovision (Nodulus).

For PL-NAc cell body inhibition experiments (Figures S3C–S3E), mice expressing NpHR/YFP in PL-NAc neurons were tested on the linear 3-chamber assay approximately 5 weeks post virus injections. Juvenile male mice were used as social targets for these experiments. The experimenter was blind to the treatment group during the course of the assay. The mice were allowed to explore the linear chamber for 3 min with no light stimulation, followed by 3 min of yellow light stimulation (594nm, 2.5-3 mW at the tip of the optical fiber) and terminating with an additional 3 min of no light. The location of the mice was tracked using Ethovision (Nodulus).

For GCaMP6f imaging experiments (Figures 4, 5, S4, and S5), all mice were imaged while exploring the arena on two consecutive visits (each visit being 10 min long): first with the social target in one location (either "social target right" or "social target left"), and next with the social target in the other location (e.g., Condition 1: social target on right, novel object on left; Condition 2: social targets mouse on left, novel object on right). The social targets were either juvenile male mice (< 6 weeks old; Figures 4 and 5), adult male mice (> 8 weeks; Figure S5C) or estrous adult females (> 8 weeks; Figure S5C). The novel objects used were either a novel toy (Figures 4 and 5) or a novel food (2g of oatmeal; Figure S5C). In a subset of the mice, in addition to imaging in the social target left and social target right conditions, mice were imaged while exploring the arena in the absence of any social targets or toys (Figures S4D and S4E) or while exploring the arena with social targets encaged at both ends (Figures S5G–S5I). The location of the mice was tracked using Ethovision (Nodulus).

Home-cage assay

On the day of the assay, mice were allowed to habituate for 30 minutes in their home-cage, following which an unfamiliar juvenile male mouse (~6 weeks, "social target") was introduced into the cage for a 5 min period. All behavior was video monitored. Social investigation was defined as periods when the imaging mouse was in pursuit (defined as the period from when the animal orients and runs toward the social target to the point when he makes contact), sniffing (defined as periods when the mouse's snout was in contact with the social target) or grooming (as periods when the forepaws of the mouse, the mouth and/or the snout region were placed gently on top of the social target) the social target. Investigations of the social target by the imaging mouse were manually annotated (using JABBA, Janelia or BORIS) (Friard and Gamba, 2016; Kabra et al., 2013). For a subset of the imaging experiments, the location of both the imaging mouse and the social target was tracked post hoc (in a semi-automated fashion using Adobe After Effects).

For PL-NAc terminal activation experiment (Figures 3A, 3B, S3A, and S3B), mice expressing ChR2 or YFP in PL-NAc terminals (ChR2 n = 10, YFP n = 8) were were allowed to investigate a novel social target introduced into his home-cage for a 5 minute period. On one of two days designated as the activation day, the mice were allowed to investigate a social target introduced into their home-cage while they were stimulated with blue light (447 nm, 1.5 mW, 5 ms long pulses at 10Hz). On the control day, mice were allowed to investigate a novel social target while being tethered, but receiving no light stimulation. Half the mice received stimulation on day 1 while the rest on day 2. The amount of time spent investigating the social target was manually annotated.

For PL-NAc cell body inhibition experiments (Figure S3F), mice expressing NpHR/YFP in PL-NAc neurons were tested on the home cage assay approximately 5 weeks after virus injections. One of the two experimental days was designated as the inhibition day and the other as control day . On the inhibition day, mice were allowed to investigate a social target introduced into their home-cage while PL-NAc neurons were inhibited with yellow light (594 nm, 2.5-3 mW). On the control day, mice were allowed to investigate a novel social target while being tethered, but receiving no light stimulation. Half the mice received light on day 1 while the rest on day 2.

For GCaMP6f imaging experiments (Figures 6 and S6), each imaging mouse was exposed to 2 social targets (stranger juvenile male mice) and a novel object presented in a random order in their home-cage.

Social conditioned place preference paradigm (Social CPP)

In this assay, on baseline day mice explored a two-chamber arena containing two empty cages at each end. Distinct walls and floors distinguished the two chambers. This was followed by 2 days of conditioning, mice were explore the arena with each chamber containing an encaged social target. On the test day mice were allowed to explore the arena in the absence of any social targets. A 10 cm arc surrounding the cages was designated as the social zone and time spent in each social zone was measured each day. The sessions lasted 20 minutes long each day.

For PL-NAc cell body inhibition experiments (Figures 7A–7E, S7A, and S7B), approximately 4 weeks post injection mice expressing NpHR/YFP in PL-NAc neurons were run on the social CPP assay. For each animal one social zone was designated as the control zone and the other zone the inhibition zone (in random). On the conditioning days, the inhibited zone was paired with yellow light stimulation (594nm, 2.5-3 mW, constant light). Light stimulation turned on when the animal moved into this zone and remained on until the animal moved out of the zone. Mice received no stimulation in the control social zone. On the test day, mice were allowed to explore the arena in the absence of light stimulation and in the absence of social targets to determine their preference for the social zones. A subset of the NpHR mice (Figures 7F and 7G; n = 5 animals), the assay was run as above but in the absence of any social targets on all days (including the conditioning days). These mice (4/5 mice, one mouse was excluded for leaving the arena multiple times during behavioral testing) were subsequently rerun on the social version of this assay a week later after establishing the absence of any spatial bias for either zone on the baseline day.

For PL-NAc cell body activation experiments (Figures 7H–7K), ~4 weeks post injection mice expressing ChR2/YFP in PL-NAc neurons were run on the social conditioned place preference paradigm. For each animal one social zone was designated as the control zone and the other zone the activation zone (in random). On the conditioning days, the stimulated zone was paired with blue light stimulation (447 nm, 1.5 mW, 5 ms long pulses at 10Hz). Blue light stimulation turned on when the animal moved into this zone and remained on until the animal moved out of the zone. Mice received no stimulation in the control social zone. On the test day, mice were allowed to explore the arena in the absence of light stimulation and in the absence of social targets to determine their preference for the social zones.

Endoscopic GCaMP6f imaging in freely moving mice

~3-4 weeks post injection, mice expressing GCaMP6f in PL-NAc neurons were acclimatized to being head-fixed and to carrying the microscope. A tethered dummy microscope was attached to the baseplate implanted on the animal for 30 minute habituation sessions across a 2-5 day period prior to the actual imaging experiment. On the day of testing, mice were left to habituate to the microscope for a 30 minutes prior to imaging. Images were acquired at 10Hz and the LED power on the scope was set between 10%–40% (0.3-2mW). A DAQ card (USB-201, Measurement computing) was used to synchronize the imaging and behavioral data.

For data analysis, the imaging data was spatially downsampled (by a factor of 2 or 4) and motion corrected with a translational correction algorithm based on cross-correlations computed on consecutive frames using the Mosaic software (Inscopix, motion correction parameters: translation only, reference image: the mean image, speed/accuracy balance: 0.1, subtract spatial mean [r = 20 pixels], invert, and apply spatial mean [r = 5 pixels]). After motion correction, the CNMFe algorithm (Zhou et al., 2016) was used to identify individual neurons, obtain their fluorescence traces and to deconvolve the fluorescence signal into firing rate estimates (tau = 1s). These firing rates were used for spatial field estimates in Figures 4D–4G, 5B, 5C, 6C, and 6D. Custom MATLAB software was used for all imaging data analysis.

QUANTIFICATION AND STATISTICAL ANALYSIS

Retrograde tracing experiments

For the data in Figure 1D, a 1-way ANOVA comparing cell density between the three PL subpopulations. For the data in Figure 1E, K–S tests were used to compare M/L distribution of the 3 populations in a pairwise manner and the p values were Bonferroni-Holm corrected.

Optogenetic and Imaging experiments

All statistical tests and data analyses were performed using MATLAB and VassarStats.net.

For PL terminal activation experiments (Figures 2, S2H, and S2I), a multifactor ANOVA, consisting of three factors: groups (ChR2, YFP), light (OFF, ON, OFF) and time epochs (first 3 minutes, middle 3 minutes, last 3 minutes) followed by a Tukey corrected post hoc tests to determine significance.

For PL-NAc cell body inhibition experiments (Figures S3C–S3E), a multifactor ANOVA, consisting of three factors: groups (NpHR, YFP), light (OFF, ON, OFF) and time epochs (first 3 minutes, middle 3 minutes, last 3 minutes) was used to determine significance.

For PL-NAc terminal activation experiment (Figures 3A and 3B), a multifactor ANOVA, consisting of groups (ChR2, YFP) and days (light, no light) as factors followed by a post hoc t tests to determine significance.

For PL-NAc cell body inhibition experiments (Figure S3F), a multifactor ANOVA, consisting of two factors: groups (NpHR, YFP) and days (Control day, Inhibition day) was used to determine significance.

For the data in Figure S6B, a 1-way ANOVA followed by post hoc Tukey HSD test was used to determine significance.

For PL-NAc cell body inhibition experiments (Figures 7A–7E), a multifactor ANOVA, consisting of two factors: groups (NpHR, YFP) and days (Baseline, Conditioning day 1, Conditioning day2, Test day) followed by a post hoc t tests comparing time spent in the each zone by the control and NpHR animals was used to determine significance.

For the data in Figure 7G, a multifactor ANOVA consisting of two factors: zones (Inhibited, Control) and days (Baseline, Conditioning day 1, Conditioning day2, Test day) was used to determine significance.

For PL-NAc cell body activation experiments (Figures 7H–7K), a multifactor ANOVA, consisting of two factors: groups (ChR2, YFP) and days (Baseline, Conditioning day 1, Conditioning day2, Test day) followed by a post hoc t tests comparing time spent in the each zone by the control and ChR2 animals was used to determine significance.

Estimating spatial fields from Ca^{2+} imaging data

To estimate spatial fields and their modulation by social investigation (Figures 4D–4G, 5B, 5C, 6C, and 6D), we used a Bayesian approach based on a Gaussian process (GP) regression model (Park et al., 2014) for calcium fluorescence imaging data. This model provides a principled statistical framework for quantifying the relationship between spatial position and neural activity.

There are several key advantages of this approach. First, it takes into account the slow dynamics of the calcium reporter so that neural activity will not be mis-attributed to the wrong location or action, as mice can travel a significant distance (or transition from social investigation to not investigation) during a single calcium transient. This also ensures that long calcium transients are not treated as providing independent samples of elevated firing, which will confound a naive shuffling-based permutation tests for significance of spatial tuning. Second, it automatically estimates the smoothness of spatial RFs using maximum likelihood, an approach known as ''maximum marginal likelihood'' (Bishop, 2006). This step is especially important for these data, given that we have no *a priori* knowledge about the smoothness of the spatial fields of PL-NAc neurons. Third, taking a Bayesian approach allows us to quantify uncertainty about the influence of each behavioral variable on neural activity (in this case, social investigation and spatial position) in the form of a posterior distribution over model parameters. This is particularly valuable in the case of social investigation data, given that behavioral parameters of interest may co-vary, and each condition is not necessarily sampled equally thoroughly (e.g., social investigation versus not investigation), which could be an issue when combined with the low rate of GCaMP transients in PL-NAc neurons. However, it is worth noting that all results reported in the paper are considered significant based on cross-validation, further ensuring that spatial selectivity estimated using this approach is robust to model mis-specification (cross validation details below).

To fit the model to data with this Bayesian approach, we discretized the field f into bins of size X ($\sim$3 cm), resulting in a discrete place field map with bins (42 bins in the linear 3-chamber assay and 247 bins in the home-cage assay). The Gaussian process places a multivariate zero-mean Gaussian prior distribution over the field, $P(\mathbf{f}) = \mathcal{N}(0,K)$, where the i,j'th element of the covariance matrix K is given by the ''gaussian'' covariance function: $K(i,j) = \boldsymbol{\rho} \exp(-||x_i - x_j||^2 / (2\delta^2))$, where x_i and x_j are the spatial location of the i'th and j'th bins of the field, respectively. This prior is governed by a pair of hyperparameters: marginal variance $\boldsymbol{\rho}$, which defines the marginal prior variance of the field elements, and length scale δ, which determines the degree of smoothness. We assume neural activity in each time bin given the animal's location follows a Gaussian distribution, $P(y(t)|\, x(t)) = \mathcal{N}(f(x(t)), \sigma^2)$, where $y(t)$ is the neural activity at time t, $x(t)$ is the animal's spatial location at time t, and the distribution over activity has mean $f(x(t))$ and variance σ^2 . We set the Gaussian process hyperparameters $\boldsymbol{\rho}$ and δ and Gaussian noise variance σ^2 by maximizing marginal likelihood, the conditional probability of the data given these hyperparameters. This allowed us to determine the optimal degree of smoothing for each field directly from the data. Then, conditioned on the hyperparameters, we used the maximum *a posteriori* (MAP) estimate to determine the field for each neuron using standard formulas for the posterior under Gaussian prior and likelihood: $\mathbf{f} = (X^T X + \sigma^2 K^{-1})^{-1} X^T Y$ where X is the design matrix, in which each row carries a 1 in the column corresponding to the spatial location of the rat in a single time bin, and the corresponding element of the column vector Y is the neural response for that time bin.

To assess the significance of each neuron's spatial selectivity in the linear 3-chamber assay (Figures 4D–4G, 5B, and 5C), a cross-validation method (based on leaving out 10% of the data) was used to compare the predicted fluorescence (based solely on the spatial field) with the actual fluorescence. Neurons were classified as having 'significant' responses when there was significant correlation between the predicted and actual fluorescence ($p < 0.05$).

For the data in Figure 4G, to determine if there were more ''spatial neurons'' and ''social neurons'' than expected by chance, the distribution of the peak activity was compared to what would be expected if peak responses followed a spatially uniform distribution. The number of neurons (from the real dataset) in each bin was compared to simulated data using a 1-tailed t test and bins with p values < 0.05 were designated as significant.

For the data in Figures 6C and 6D, the imaging and behavioral data were concatenated across exposure of two social target mice. To determine if adding social investigation as a parameter improved our prediction of the activity of each neuron, we compared two models. One model was based on neurons having the same spatial field regardless of whether or not the mice was interacting (spatial-only model), and the other model was based on calculating a different spatial field during investigation versus during non-investigation epochs (social+spatial model; smoothness parameters were determined from the entire dataset). Cross-validation (based on leaving out 10% of the data) was used to determine how the predicted fluorescence based on each model compared to the actual fluorescence. Correlation coefficients comparing the predicted and actual fluorescence were generated for each neuron and for both models. A paired t test was then used to compare the correlation coefficients generated by the two models. In Figure 6E,

neurons were classified as 'significant' when at least one of the three models resulted in significant correlation between the predicted and actual fluorescence ($p < 0.05$). Significant neurons were then classified as "social," "social+spatial" or "spatial" based on which model led to the greatest correlation coefficient with cross-validation.

DATA AND SOFTWARE AVAILABILITY

The accession number for the RNA seq data from Figure 1 examining differences between the PL-NAc, PL-VTA and PL-Amyg neurons is GEO: GSE104943. MATLAB code for estimating spatial fields using GP regression is available at https://github.com/wittenlab/Spatial-field-estimates-Murugan-et-al-Cell-2017#gp-regression-for-place-field-estimation.

Cell

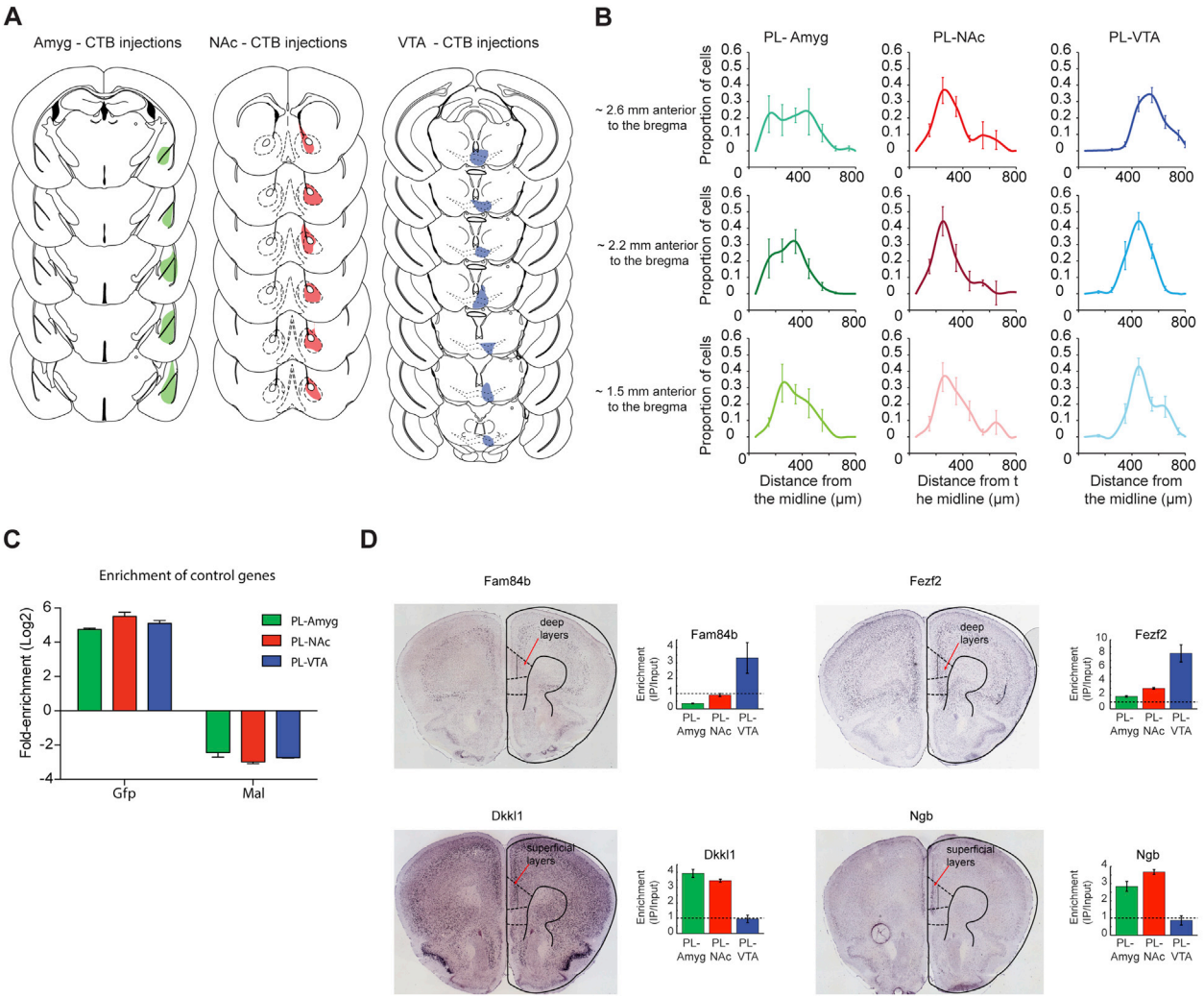

Figure S1. PL Neurons Projecting to the NAc, VTA, and Amyg Are Anatomically and Molecularly Distinct, Related to Figure 1

(A) Reconstructions of injection sites (determined by maximal spread) in mice injected with CTB in the Amyg (A; green), NAc (B; red) and the VTA (C; blue).

(B) Distribution of PL-Amyg (left column, shades of green), PL-NAc (middle column, shades of red) and PL-VTA (right column, shades of blue) projection neurons along the anterior- posterior axis (top row: ~2.6 mm anterior to bregma, middle row: ~2.2 mm anterior to bregma and bottom row: ~1.5 mm anterior to the bregma). Error bars denote SEM.

(C) Enrichment of the positive control marker *Gfp* and a depletion of the glial cell marker Mal was observed across all three PL subpopulations. Fold enrichments (IP/Input) are on a Log2 scale.

(D) Using the Allen Brain atlas, we confirmed that several differentially expressed genes that we identified (*Fam84b*, *Fezf2*, *Ngb*, and *Dkkl1*; 1-way ANOVA, $p < 0.01$ for all 4 genes) exhibited the laminar expression patterns predicted based on the enrichment data and our anatomical characterization in Figure 1E. Data are presented as mean ± SEM.

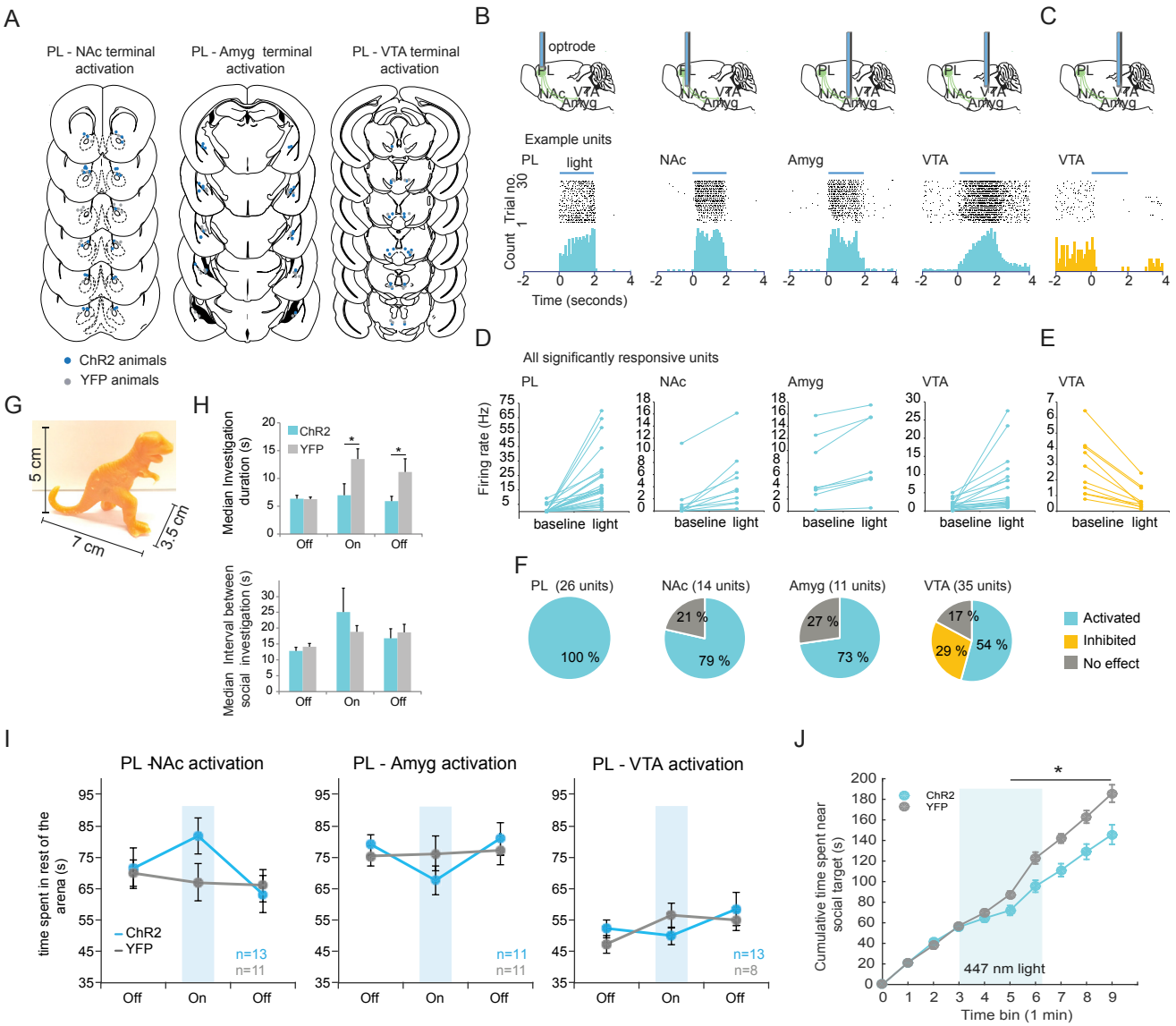

Figure S2. Histological and Electrophysiological Confirmation of ChR2-Mediated Activation of PL Terminals in the NAc, Amyg, and VTA, Related to Figure 2

(A) Histological reconstruction of optical fiber tip placements in PL-NAc (left), PL-Amyg and PL-VTA mice. Blue dots: ChR2, gray dots: YFP.

(B) Example units from *in vivo* extracellular recording of light-evoked action potentials (473 nm, 2 s, 30 trials) in the PL, NAc, Amyg and VTA of mice injected with AAV5-CaMKIIa-hChR2-EYFP in PL. Top row: schematic of the recording configuration, optrode inserted in the PL. Middle row: Raster plot showing action potentials of an example units in PL, NAc, Amyg and VTA in responding to 30 consecutive trials of light illumination. Bottom row: A histogram of the spikes binned every 100 ms.

(C) An example VTA unit inhibited by stimulation of PL terminals expressing ChR2.

(D) Population summary of firing rate changes of all PL, NAc, Amyg and VTA units recorded that showed significant increases from the baseline (PL: $p < 0.0001$, NAc: $p = 0.003$, Amyg: $p = 0.004$, VTA: $p = 0.005$, for paired two tailed t test comparing mean firing rate across epochs).

(E) Population summary of firing rate changes of units in the VTA that showed significant decreases in their firing rate during stimulation of ChR2 expressing PL terminals ($p = 0.006$, Paired two tailed t test).

(F) Percentage of PL, NAc, Amyg and VTA units excited (blue), inhibited (yellow) or not affected (gray) by light stimulation.

(G) The novel objects used in the study were plastic toys roughly 7x3.5x5cm in dimensions.

(H) Top panel: Activation of PL-NAc terminals decreased the duration of social investigation bouts and this effect persists after light was turned off. (ANOVA with group, epoch, and light as factors; $p = 0.049$, ANOVA group X light interaction). Bottom panel: The activation of PL-NAc terminals had no effect on the intervals between social investigation bouts ($p = 0.505$, ANOVA group X light interaction).

(I) Activating PL-NAc (left), PL-Amyg (middle) and PL-VTA (right) terminals had no effect on time spent in rest of the arena ($p = 0.199$ for Group X light for PL-NAc, $p = 0.689$ for PL-Amyg and $p = 0.117$ for PL-VTA).

(J) In the 3-chamber assay, the decrease in time spent in the vicinity of the social target with activation of PL-NAc terminals becomes significant after 2 minutes of stimulation and is most different after 3 minutes of stimulation ($p < 0.05$, two-tailed t test on each minute of data). Data are presented as mean ± SEM.

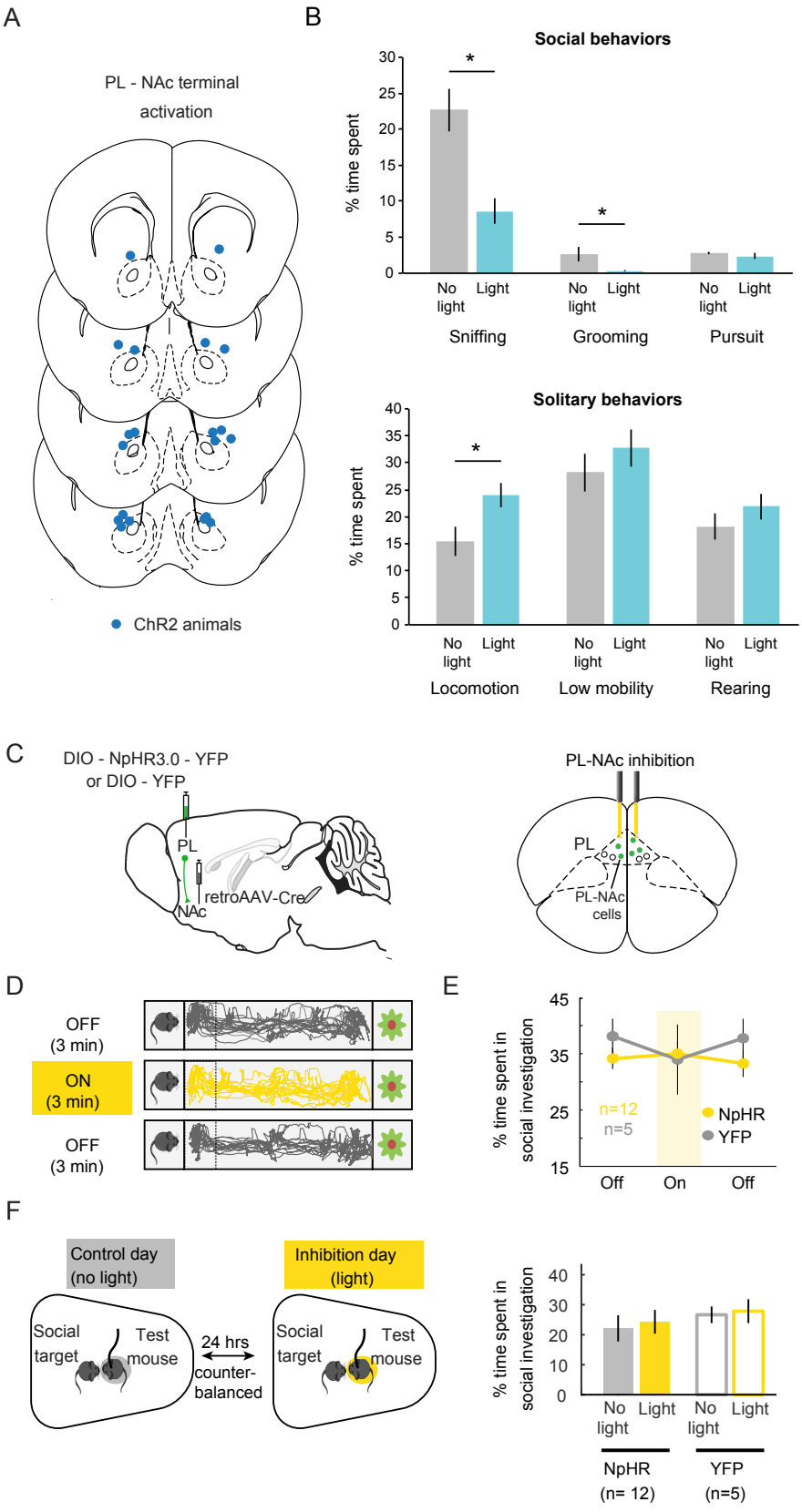

(legend on next page)

Figure S3. Activation, but Not Inhibition, of PL-NAc Neurons Decreases the Amount of Time Spent in Social Investigation, Related to Figure 3

(A) Histological reconstruction of optical fiber tip placements in the PL-NAc mice, (blue dots: ChR2, n = 10 animals).

(B) Top: Activation of ChR2 expressing PL-NAc terminals decreased the amount of time mice spent in sniffing and grooming a social target mouse but had no effect on the time spent in pursuit of the social mouse (two-tailed paired t test comparing time spent in each behavior during light on versus light off; Sniffing: $p = 0.0013$, Grooming: $p = 0.051$, Pursuit: $p = 0.27205$). Bottom: Activation of ChR2 expressing PL-NAc terminals increased the amount of mice spent locomoting but had no effect on the time the mouse engaged in other solitary behaviors such as periods of low mobility and rearing (Locomotion: $p = 0.04402$, Low mobility: $p = 0.338877$, Rearing: $p = 0.287691$).

(C) Left: To target NpHR expression to PL-NAc neurons, the retrograde virus retroAAV-Cre was injected in the NAc and Cre-dependent AAV5-DIO-NpHR or AAV5-DIO-YFP was injected in PL. Right: Schematic of fiber placement in PL.

(D) Position tracking from a representative mouse receiving inhibition of PL-NAc neurons while exploring the 3-chamber arena during pre-inhibition (top panel), inhibition (middle panel, 594 nm yellow light 2-3 mW) and post-inhibition (bottom panel).

(E) Inhibition of PL-NAc neurons had no effect on time spent in proximity of the social target ($p = 0.397$ for group X light, 2-way ANOVA).

(F) Left: Schematic of the home-cage assay. Right: Spatially nonspecific inhibition of PL-NAc neurons had no effect on the time mice spent in social investigation ($p = 0.825$ for group X light, 2-way ANOVA).

Data are presented as mean ± SEM.

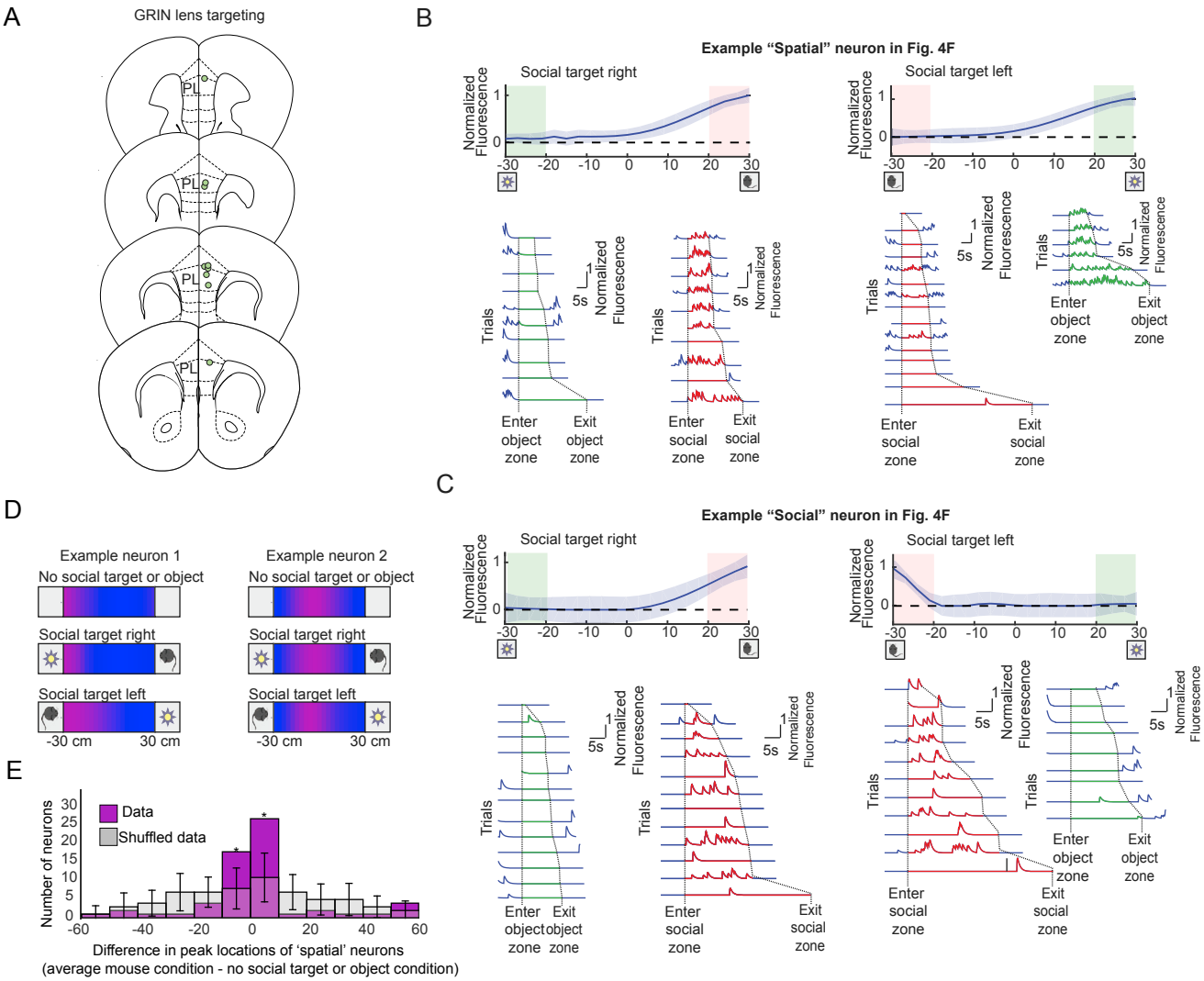

Figure S4. Characterizing Spatial and Social Responses of PL-NAc Neurons, Related to Figure 4

(A) Histological reconstruction of GRIN lens tip placements in the PL of mice expressing GCaMP6f in PL-NAc projection neurons (green dots, n = 9 animals).

(B) Example spatial neuron in Figure 4F. Top: Response field with error bars (2 standard deviations) and Bottom: trial by trial responses in the object zone (green) and social zone (red).

(C) Example social neuron in Figure 4F. Response field with error bars (top) and trial by trial responses (bottom).

(D) Example "spatial neurons" that exhibited peak responses at a similar spatial location across all three conditions (no social target or object condition on top, social target right condition in the middle and social target left condition on the bottom).

(E) Population summary: Histogram of difference in location of peak response across the mouse/target conditions and the no social target/object condition reveals that more neurons had stable peak responses than expected by chance ($p < 0.001$, 1 tailed t test comparing data in each bin to simulated data generated from a spatially uniform peak distribution; error bars are 2 standard deviations).

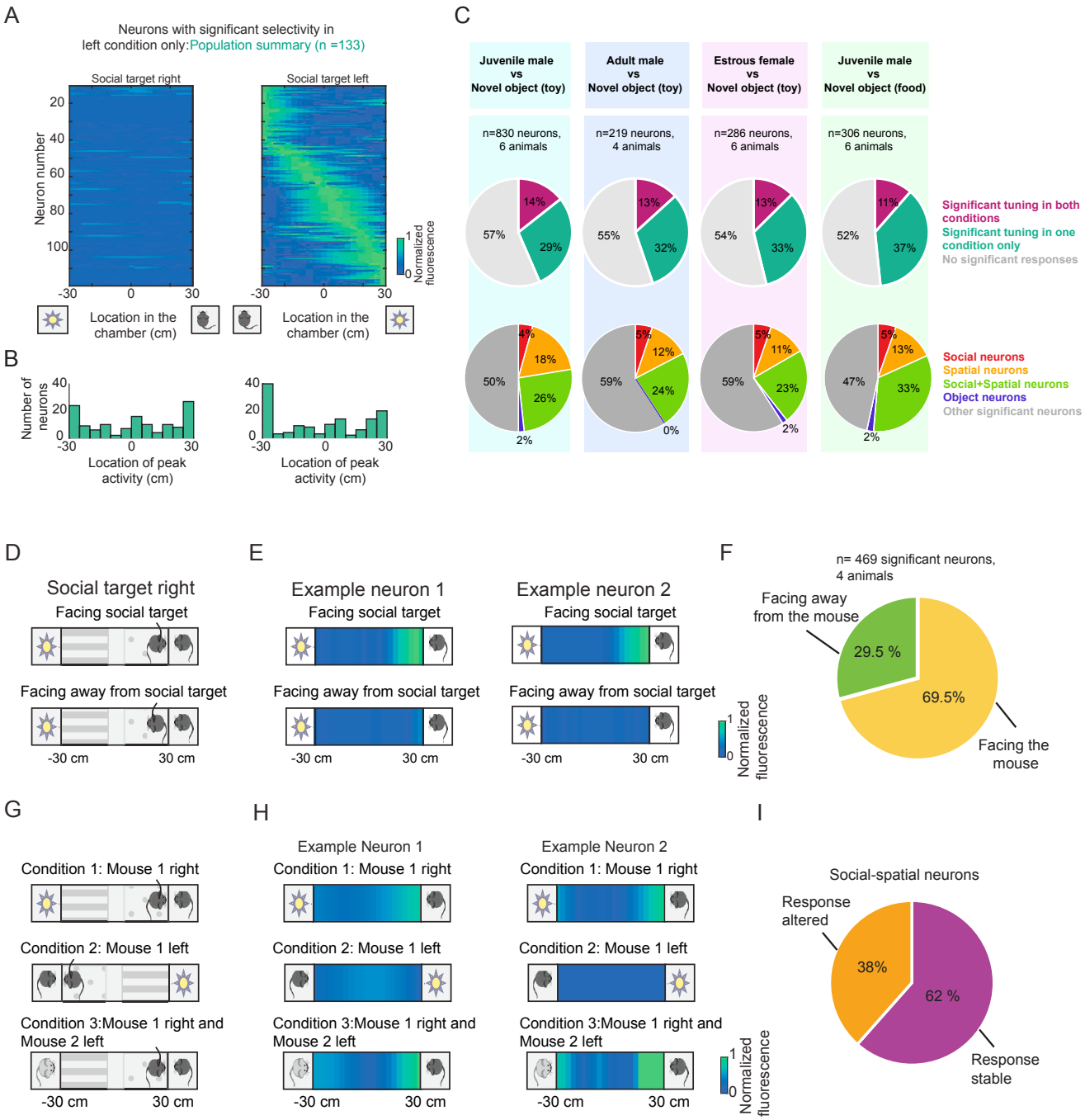

Figure S5. Characterizing PL-NAc Activity in the Linear 3-Chamber Assay, Related to Figure 5

(A) Spatial fields of all neurons with significant responses (n = 133) only in the social target left condition (right panel) and not the social target right condition (left panel).

(B) Histogram of the peak responses of neurons along the length of the chamber showing many neurons responding in the proximity of the social target in the social target left condition (right panel), while no distinction between the social target and novel object was observed in the non-preferred social target right condition (left panel).

(C) Comparing PL-NAc responses to the various social targets (juvenile male, adult male, estrous female), novel objects (toy, food). Top row: A similar fraction of neurons that were active in neither, both, or only one condition. Bottom row: Of the neurons with significant responses, similar fractions of neurons were classified as social, spatial, social-spatial or object neurons regardless of the social target or novel object used.

(D) For every neuron, two spatial fields were calculated: one based on the subset of time when the imaged mouse was oriented toward the social target, and the other based on time when it oriented away from the social target. This provided significantly greater predictive power than a model with only 1 field per neuron.

(legend continued on next page)

(E and F) Example neurons and population summary show that neurons responded more strongly when the imaged mouse was oriented toward rather than away from the social target.
(G) PL-NAc neurons (n = 153 neurons from 4 mice) were imaged in 3 conditions, Condition 1: target mouse 1 right & novel object left, Condition 2: target mouse 1 left & novel object right and Condition 3: target mouse 1 right & target mouse 2 left. Social-spatial neurons were identified as those that responded in the proximity of the social target only in condition 1 and not 2 (or vice versa, see Figure 5).
(H) Example social-spatial neurons that remained stable in condition 3 when the additional social target was introduced in the other location.
(I) A majority of the social spatial neurons that remained stable (62%) while a smaller fraction (38%) was sensitive to the presence of the 2nd social target in condition 3, and not only the 1st.

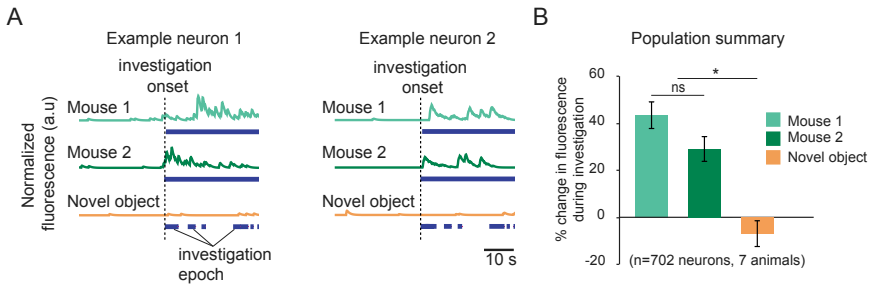

Figure S6. PL-NAc Neurons Respond More Strongly to Social Target Investigation than to Novel Object Investigation in the Home-Cage Assay, Related to Figure 6

(A) Example neurons with elevated activity during social investigation of multiple social targets (traces in green) but not during the investigation of a novel object (orange).

(B) Across the population (n = 702 neurons, n = 7 mice), neural responses were greater than baseline during investigation of the social target but not novel object ($p < 0.0001$, for 1-way ANOVA with investigation of mouse 1, mouse 2, versus novel object as the factor, post hoc Tukey HSD tests; $p = 0.155$ for mouse1 versus mouse 2, $p < 0.001$ for mouse 1 versus novel object, $p < 0.001$ for mouse 2 versus novel object). Error bars denote SEM.

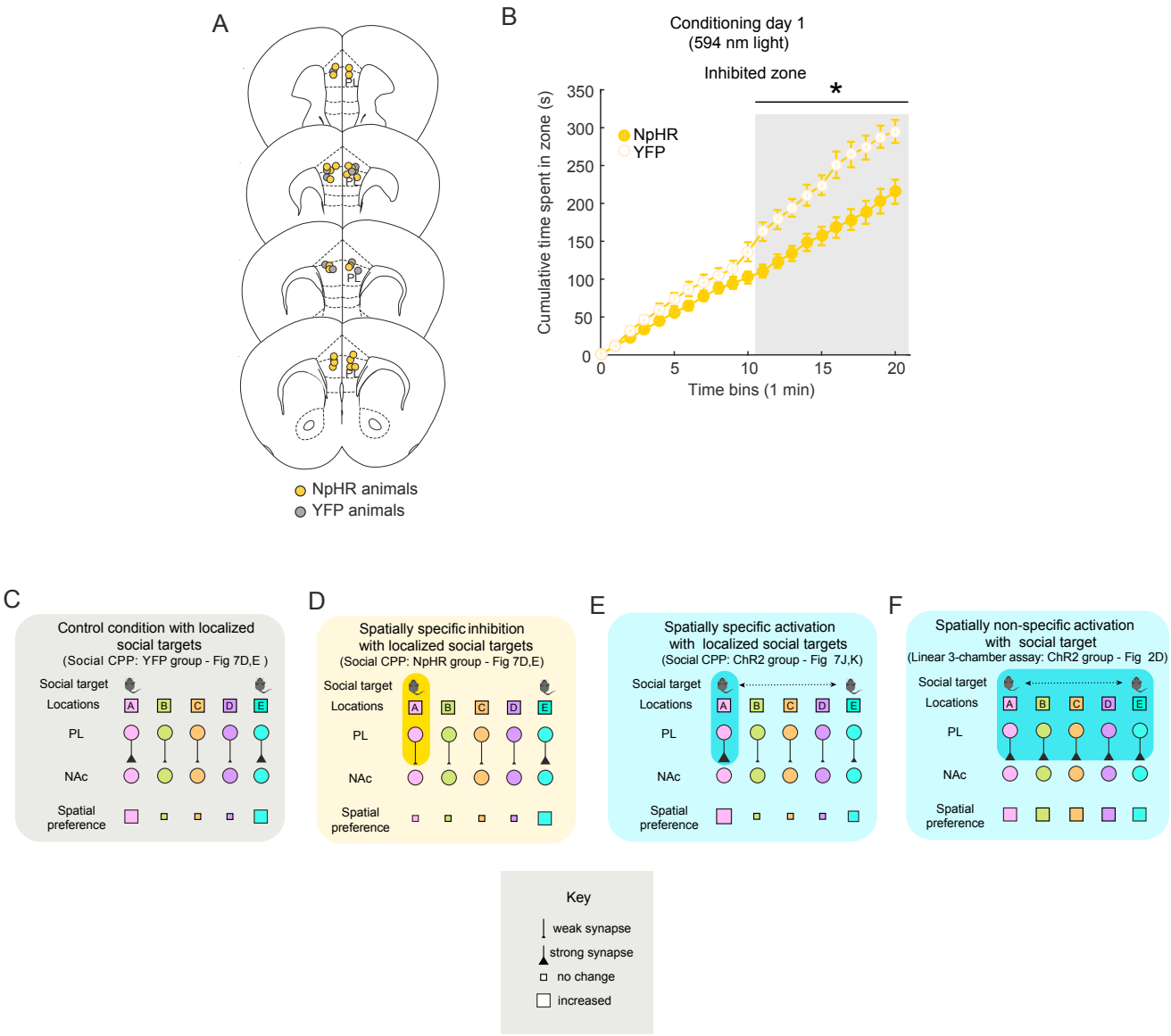

Figure S7. PL-NAc Neurons Bidirectionally Modulate Social-Spatial Learning, Related to Figure 7

(A) Histological reconstruction of optical fiber tip placements in the PL-NAc mice, (yellow dots: NpHR, n = 12 animals, gray dots: YFP, n = 5).

(B) The difference in time near the social target emerged gradually between PL-NAc NpHR mice and YFP control mice in the social CPP experiment. This difference is significant only after 11 minutes on conditioning day 1 ($p < 0.05$, two-tailed t test on each 1 min bin). Error bars denote SEM.

(C–F) In all panels, PL-NAc neurons are active during social investigation in a specific location (location A, B, C, D, or E). The strength of the synaptic connection between a PL neuron and its target in NAc increases during social investigation for the PL neuron that encodes that location. The strength of the PL-NAc synapse determines the mouse's spatial preference for the corresponding spatial location. (C) In this case (YFP control group in Figures 7D and 7E), there is a target mouse in location A and E. Therefore, synaptic connections of PL-NAc neurons that respond during social investigation in those locations are strengthened, leading to an increase in preference for both location A and E. (D) Same as (C), but the PL-NAc neurons that respond in location A are silenced (NpHR group from Figures 7D and 7E). In this case, synaptic connection of location A neurons are not strengthened, but location E neurons are strengthened. (E) Same as (C), but PL-NAc neurons were selectively activated in location A but not E (ChR2 group from Figures 7J and 7K). In this case, synaptic connection of location A neurons are strengthened leading to an increase in the preference for location A. (F) Spatially nonspecific excitation may instead strengthen PL-NAc synapses, regardless of location (Figures 2D and 3B). This may effectively increase the relative preference for non-social locations.